










Cite this: *Nanoscale Horiz.*, 2022, 7, 141

## Applications of liquid metals in nanotechnology

Francois-Marie Allieux, <sup>a</sup> Mohammad B. Ghasemian, <sup>a</sup> Wanjie Xie, <sup>a</sup> Anthony P. O'Mullane, <sup>b</sup> Torben Daeneke, <sup>c</sup> Michael D. Dickey <sup>d</sup> and Kourosh Kalantar-Zadeh <sup>\*a</sup>

Post-transition liquid metals (LMs) offer new opportunities for accessing exciting dynamics for nanomaterials. As entities with free electrons and ions as well as fluidity, LM-based nanomaterials are fundamentally different from their solid counterparts. The low melting points of most post-transition metals (less than 330 °C) allow for the formation of nanodroplets from bulk metal melts under mild mechanical and chemical conditions. At the nanoscale, these liquid state nanodroplets simultaneously offer high electrical and thermal conductivities, tunable reactivities and useful physicochemical properties. They also offer specific alloying and dealloying conditions for the formation of multi-elemental liquid based nanoalloys or the synthesis of engineered solid nanomaterials. To date, while only a few nanosized LM materials have been investigated, extraordinary properties have been observed for such systems. Multi-elemental nanoalloys have shown controllable homogeneous or heterogeneous core and surface compositions with interfacial ordering at the nanoscale. The interactions and synergies of nanosized LMs with polymeric, inorganic and bio-materials have also resulted in new compounds. This review highlights recent progress and future directions for the synthesis and applications of post-transition LMs and their alloys. The review presents the unique properties of these LM nanodroplets for developing functional materials for electronics, sensors, catalysts, energy systems, and nanomedicine and biomedical applications, as well as other functional systems engineered at the nanoscale.

Received 12th November 2021,  
Accepted 23rd December 2021

DOI: 10.1039/d1nh00594d

rsc.li/nanoscale-horizons

<sup>a</sup> School of Chemical Engineering, University of New South Wales (UNSW), Sydney, NSW 2052, Australia. E-mail: k.kalantar-zadeh@unsw.edu.au

<sup>b</sup> School of Chemistry and Physics, Queensland University of Technology (QUT), Brisbane, QLD 4001, Australia

<sup>c</sup> School of Engineering, RMIT University, Melbourne, Victoria, 3001, Australia

<sup>d</sup> Department of Chemical and Biomolecular Engineering, North Carolina State University, 911 Partners Way, Raleigh, NC, 27695, USA

### 1. Introduction

Mercury (Hg) is traditionally the most recognized liquid metal (LM) that remains a liquid well below room temperature (melting point:  $-38.8$  °C). However, due to its high toxicity,



**Francois-Marie Allieux**

*Francois-Marie Allieux is a postdoctoral fellow at the School of Chemical Engineering, University of New South Wales (UNSW), Sydney, Australia. He completed his PhD in Material Science in 2017 at Deakin University, Geelong, Australia. Prior to that, Dr Allieux received his Master of Chemical Engineering from the Paul Sabatier University in Toulouse, France. Dr Allieux's research interests include the fundamental and applications of low-melting point and liquid metals for environmental processes and technologies. His current research focuses on the formation of liquid metal nanostructures.*



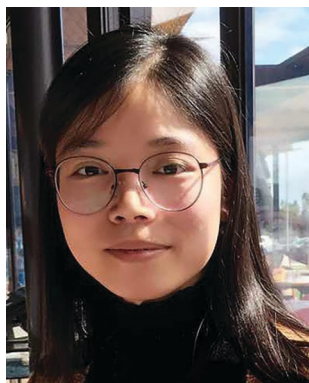
**Mohammad B. Ghasemian**

*Mohammad Bagher Ghasemian is a postdoctoral fellow in the Center for Advanced Solid and Liquid based Electronics and Optics (CASLEO) in the School of Chemical Engineering, University of New South Wales (UNSW), Australia. He received his PhD degree in Materials Science & Engineering from UNSW in 2018. Dr Ghasemian's research interests include the fundamentals and applications of liquid metals in 2D materials, piezoelectric materials, sensors, and additive manufacturing.*

high vapor pressure, and low boiling point (356.7 °C), Hg is being increasingly phased out for most industrial, consumer or research applications. Other near room temperature melting point LMs include the highly pyrophoric rubidium (Rb, melting point: 39.3 °C) and caesium (Cs, melting point: 28.4 °C). Therefore, research on LMs is now more than ever centered around the low melting point post-transition metal gallium (Ga), which has a melting point of 29.8 °C. Unlike liquid Hg, liquid Ga presents unusual properties due to the high degree of covalent bonding within the bulk of its LM matrix, which results in it staying in the liquid state over a range of 2000 °C. It also has a low vapor pressure below 1500 °C.<sup>10–12</sup> At near room temperature, the effectively zero vapor pressure allows for safe and routine operation in common research environments and also

applications in high vacuum environments.<sup>21</sup> To expand the family of LMs, research is now expanding from that of Ga and Ga alloys to other post-transition metals including indium (In, melting point: 156.6 °C), tin (Sn, melting point: 231.9 °C) and bismuth (Bi, melting point: 271.4 °C) that all melt below 330 °C.<sup>21</sup> Cadmium (Cd, melting point: 321.1 °C), thallium (Tl, melting point: 304.0 °C) and lead (Pb, melting point: 327.5 °C) are also considered in this family of low melting point post-transition metals but, due to their high toxicity, are often not incorporated in general research areas and applications.

The bulk structure of low melting point post-transition LMs and their alloys is particularly hard to characterize as they are dense and impermeable to many characterization techniques.



**Wanjie Xie**

*Wanjie Xie completed her PhD in 2020 at Deakin University, Australia. She then became a postdoctoral researcher at the School of Chemical Engineering, University of New South Wales (UNSW), Australia, where she focused on investigating the synthesis of functional nanocomposites based on gallium-based liquid metals.*



**Anthony P. O'Mullane**

*Anthony O'Mullane received his BSc Chemistry degree (1997) and PhD degree (2001) from University College Cork (Ireland). He is a Fellow of the Royal Society of Chemistry, the Royal Australian Chemical Institute and Queensland Academy of Arts and Sciences. He is the immediate past-Chair of the Electrochemistry Division of the RACI and served as vice chair of the Physical Electrochemistry Division of the International Society of Electrochemistry. He is an Editorial Board Member of ChemElectroChem. His work focuses on the electrochemical fabrication, characterisation and application of a wide range of materials including liquid metals with energy and environmental remediation applications.*



**Torben Daeneke**

*Torben Daeneke received his PhD in Chemistry from Monash University, Australia in 2012. After graduating he held postdoctoral appointments at the CSIRO and at RMIT University (Australia). In 2018 he joined RMIT's School of Engineering as a faculty member where he is now an Associate Professor. Dr Daeneke has authored over 100 peer-reviewed journal articles and has been awarded several fellowships and grants, including an ARC*

*Discovery Early Career Researcher Award (DECRA) and a RMIT VC postdoctoral fellowship. His research focuses on studying the chemistry of liquid metals, the synthesis of 2D materials and the development of novel catalysts.*



**Michael D. Dickey**

*Michael Dickey received a BS in Chemical Engineering from Georgia Institute of Technology (1999) and a PhD from the University of Texas (2006) under the guidance of Professor Grant Willson. From 2006–2008 he was a post-doctoral fellow in the lab of Professor George Whitesides at Harvard University. He is currently the Camille and Henry Dreyfus Professor in the Department of Chemical & Biomolecular Engineering at NC State University. He completed a sabbatical at Microsoft in 2016. Michael's research interests include soft matter (liquid metals, gels, polymers) for soft and stretchable devices (electronics, energy harvesters, textiles, and soft robotics).*

Bulk LMs present a matrix lacking any crystalline features formed of free ions and electrons, which provide metallic behavior including high thermal and electrical conductivity and also a water-like viscosity.<sup>32</sup>

Surface layering phenomena, which correspond to an atomic-scale ordering in the interfacial top layers, can occur in post-transition LMs and alloys. The study of the surface structure and composition of Ga and Ga-based LMs have been the subject of numerous investigations using advanced reflectivity, scattering techniques and nanotopography assessments.<sup>10,11,34</sup> The surface of Ga and Ga-based LMs have been demonstrated to be composed of an atomically smooth surface comprised of a sea of quasi-free electrons and positive ions.<sup>11,35,36</sup> Despite having an atomically smooth surface free of any crystalline structure, liquid Ga has been shown to possess a lamellar ordered surface, which is a few atomic diameters thick.<sup>10,11,35</sup> However, differences between LMs also exist, for instance, liquid Ga presents localized electrons in the bulk matrix as opposed to liquid In, which shows more uniformly distributed free electrons.<sup>37</sup> Liquid Sn was also reported to exhibit such atomic surface layering.<sup>38</sup> In addition, liquid Ga, and many of its most common liquid alloys, in air at ambient conditions, establishes an atomically thin self-limiting oxide layer following a Mott–Cabrera model that is often reported to be between 0.5 and 3 nm thick.<sup>39,40</sup> In contrast, the oxide layers of liquid In, Sn and Bi grow into thicker coatings when exposed to oxygen.<sup>41–44</sup>

LMs and their alloys can be synthesized at the nanoscales using various agitation methods. Nanoparticles composed of at least two different metallic elements are typically referred to as nanoalloys.<sup>45</sup> Liquid nanoalloys can be used for the synthesis of different solid, liquid and liquid/solid nanostructures such as core/shell, stratified, high and low entropy and fully phase separated nanoparticles.<sup>14,23,28</sup> LM-based nanoalloys have been integrated into nanocomposites of organic and inorganic materials, which properties have been explored in polymeric matrices and also their interactions with biomaterials have been investigated.<sup>3,17,20,46,47</sup> Altogether multi-elemental nanocompounds and nanocomposites, made of LMs, have been shown to offer interesting physical and chemical properties that originated from the liquid state of these entities.



**Kourosh Kalantar-Zadeh**

*Kourosh Kalantar-Zadeh is a professor of Chemical Engineering at the University of New South Wales (UNSW), Sydney, Australia. He is involved in research in the fields of materials sciences, electronics, and transducers. He is best known for his works on two-dimensional semiconductors, ingestible sensors and liquid metals. He led his group to the invention of an ingestible chemical sensor: human gas sensing capsule.*

Finally, the incorporation of nano-sized liquid particles is rapidly emerging in exciting applications. Their utilization has been shown to enhance catalytic activity, provide the possibility of self-healing in electronics, improve sensing (mechanical, gas, and biological), and harvest energy. They have also been used in nanomedicine and biotechnology, *e.g.* for drug delivery and targeting applications with responses that are not seen in solid nanoparticles.

This review aims at providing insights into how low melting point post-transition LMs and alloys influence nanotechnology. The methods utilized for the formation of LM-based nanostructures and nanoparticles are presented. The review discusses multi-elemental LM nanodroplets and their solidification, which relates to their entropy and environmental stimuli. The reactivity, surface composition, interfacial layering and nanodomains at the dynamic surface of LM alloys are also reported. The very recent and emerging applications of LMs for the synthesis of nanomaterials, energy production and storage, electronics, sensing, catalysis and in nanomedicine are then presented. Finally, some future prospects for the application of LMs in nanotechnology are discussed.

## 2. Characteristics of post-transition metals and alloys at the nanoscale

### 2.1 Post-transition metals and alloys

Post-transition metals share common properties such as low melting point, electrical conductivity, mixed metallic and covalent bonds, and are softer compared to transition metals. However, a universal definition for post-transition metals remains only partially accepted. Fig. 1a shows the group of elements defined as post-transition metals considered in this review with the addition of the elements in the zinc group due to their importance in this review. In a similar way to transition metals, post-transition metals also form a multitude of alloys. Alloying of post-transition metals forms low melting point alloys with tunable properties and phase compositions. In addition, post-transition metals also form eutectic alloys in the liquid state, which have melting points lower than their respective single elements. For instance, a eutectic binary alloy formed of 75.0 wt% Ga and 25.0 wt% In (EGaIn) has a melting point of 15.6 °C, which is lower than the respective melting points of each element. Another example of a post-transition eutectic alloy is Galinstan, which has a reported melting point of around ~10 °C, and is a ternary alloy of 68.5 wt% Ga, 21.5 wt% In, and 10.0 wt% Sn.<sup>48</sup> A plethora of other eutectic binary alloys of relatively low temperature melting points can be formed from post-transition metals such as EBiSn (57 wt% Bi and 43 wt% Sn, melting point 139.8 °C), and ternary alloys, including Field's metal (51 wt% In, 32.5 wt% Bi, 16.5 wt% Sn, melting point 62 °C), and even quinary alloys that include Pb and/or Cd elements.<sup>23,28,32</sup> The representative eutectic post-transition metal alloys are presented in Table 1.

Post-transition metals are now increasingly considered as universal platforms for alloying with other metallic elements

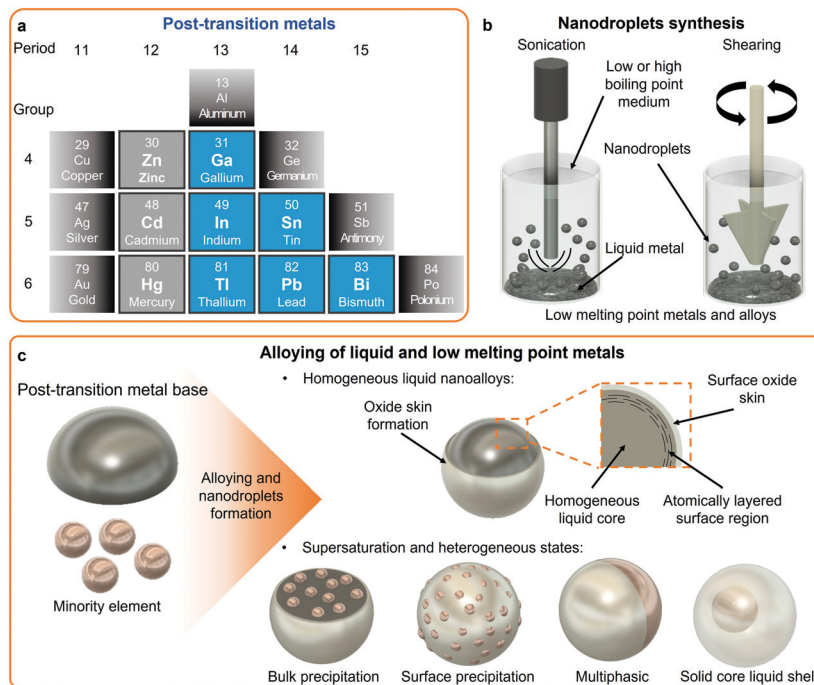


**Fig. 1** (a) Portion of the periodic table showing the elements defined as post-transition metals (in blue) and zinc group (in gray) due to the importance to this paper. (b) Representation of the sonication and shearing methods used for the synthesis of LM nanodroplets from low melting point metals and alloys. (c) Illustration of the surface oxide and atomic layering phenomena in LMs and the reported nanostructure variations in LM nanodroplets.

**Table 1** Composition of some important low melting point post-transition eutectic alloys

Alloy name	Eutectic composition (wt%)	Eutectic melting point (°C)	Density (g cm <sup>-3</sup> )
EGaIn	Ga <sub>78</sub> In <sub>22</sub>	15.5	6.28
EGaSn	Ga <sub>86.5</sub> Sn <sub>13.5</sub>	20.5	—
EBiCd <sup>a</sup>	Bi <sub>60</sub> Cd <sub>40</sub>	146.0	10.49
EBiSn	Bi <sub>57</sub> Sn <sub>43</sub>	139.0	8.12
EBiIn	Bi <sub>49</sub> In <sub>51</sub>	68.1	6.34
EBiPb <sup>a</sup>	Bi <sub>55.5</sub> Pb <sub>44.5</sub>	125.5	10.52
ECdIn <sup>a</sup>	Cd <sub>25.6</sub> In <sub>74.4</sub>	126.0	—
ECdPb <sup>a</sup>	Cd <sub>17.5</sub> Pb <sub>82.5</sub>	246.0	10.40
ECdSn <sup>a</sup>	Cd <sub>32.3</sub> Sn <sub>67.7</sub>	176.0	7.68
ECdTl <sup>a</sup>	Cd <sub>17</sub> Tl <sub>83</sub>	203.5	11.35
EPbSn <sup>a</sup>	Pb <sub>37</sub> Sn <sub>63</sub>	183.0	8.40
ESnTl <sup>a</sup>	Sn <sub>57</sub> Tl <sub>43</sub>	166.0	8.59
EGaSnZn <sup>53</sup>	Ga <sub>86</sub> Sn <sub>11</sub> Zn <sub>3</sub>	14.9	6.14
EBiPbSn <sup>a</sup>	Bi <sub>52.5</sub> Pb <sub>32</sub> Sn <sub>15.5</sub>	95.0	9.69
Galinstan	Ga <sub>68.5</sub> In <sub>21.5</sub> Sn <sub>10</sub>	~10.0	6.44
Field's metal	Bi <sub>32.5</sub> In <sub>51</sub> Sn <sub>16.5</sub>	62.0	7.88
Wood's metal <sup>a</sup>	Bi <sub>50</sub> Pb <sub>26.7</sub> Sn <sub>13.3</sub>	70.0	9.67
GaSnZn + In <sup>54</sup>	EGaSnZn + In <sub>21.4</sub>	15.9	6.20
EBiPbInSn <sup>a</sup>	Bi <sub>49</sub> Pb <sub>18</sub> In <sub>21</sub> Sn <sub>12</sub>	58.0	8.58
Cerrow 117 <sup>a</sup>	Bi <sub>44.7</sub> Pb <sub>22.6</sub> Sn <sub>8.3</sub> Cd <sub>5.3</sub> In <sub>19.1</sub>	47.2	8.86

<sup>a</sup> Eutectic alloy containing toxic metals (Pb, Cd and Tl), In is considered less toxic in comparison.

including other post-transition, transition, and alkali metals, and also rare earth elements.<sup>21,32,49</sup> Considering the concept of high entropy alloys, elemental combinations of post-transition metals and their resulting structures are nearly limitless. LM alloys can form liquid monophasic and multiphasic liquid–solid alloys. Elements in liquid monophasic alloys are homogeneously

distributed within the LM matrix as opposed to multiphasic alloys, where segregated solid domains exist in various forms. The low melting points of the post-transition metals provide facile paths for the synthesis of nanoalloys and multi-elemental nanoparticles using a variety of processes applied to the alloy melts. Despite all these possibilities, systematic alloying of post-transition metals based on well-designed elemental libraries and the study of their nanostructures remain largely unexplored.

## 2.2 Surface chemistry of post-transition LMs and alloys and surface layering

Single and multi-elemental LM phases exhibit extraordinary surface enrichment phenomena which are increasingly becoming recognized for the synthesis of nanostructured materials.<sup>50</sup> In LM matrices, it is understood that elements naturally compete to appear at the surface of LMs. Therefore, the surface composition might vary dramatically in comparison to the bulk. As an example, Ga-based LMs form a self-limiting passivating oxide skin layer, the composition of which is determined by the makeup of the Ga-based alloy and conditions of the environment at the interface with the LM.<sup>50</sup> Typically in the air, the oxide skin layer of LMs such as Ga, EGaIn or Galinstan is composed of amorphous gallium oxide (Ga<sub>2</sub>O<sub>3</sub>).<sup>51</sup> However, alloying with other elements in the bulk LM can drastically change the elemental composition of the oxide layer. For example, when very small amounts (~1 wt%) of aluminum (Al), gadolinium (Gd) or hafnium (Hf) are mixed with Ga, the surface of the liquid Ga is occupied with their oxides, namely aluminum oxide (Al<sub>2</sub>O<sub>3</sub>), gadolinium oxide (Gd<sub>2</sub>O<sub>3</sub>)

and hafnium oxide (HfO<sub>2</sub>), respectively, rather than Ga<sub>2</sub>O<sub>3</sub>, indicating the higher tendency of Al, Gd and Hf for enriching the surface of the alloy as compared to Ga.<sup>50</sup> The surface composition follows the preferential oxide formation of the alloyed materials that offer the lowest Gibbs free energy for oxide formation.<sup>50,52</sup>

Indium tin oxide (ITO) sheets were also synthesized and collected through a squeeze-print process from the surface of InSn liquid alloys confirming the contribution of both In and Sn in the surface layer. However, the ratios of In/Sn in the collected sheets differed significantly from their initial ratios in the bulk. Sn showed a higher tendency than In to migrate to the surface and contribute to the oxide layer.<sup>55</sup> This competitive elemental migration from the core to the surface of liquid alloys can selectively dope such 2D metal oxides. By using liquid alloys with various ratios of Bi and Sn, it is possible to obtain Bi<sub>2</sub>O<sub>3</sub> doped 2D SnO. Sn showed much stronger preference than Bi for migration to the interface of liquid alloys, even at very low Sn concentrations. In this case, Bi<sub>2</sub>O<sub>3</sub>-doped SnO nanosheets with the highest atomic percentage of 0.7% for Bi were collected from the surface of liquid alloys while the atomic percentage of Bi in the bulk alloy was around 90%.<sup>56</sup> Melts of Bi alloys can also show preferential oxidation phenomenon. As an example, the formation and collection of antimony oxide (Sb<sub>2</sub>O<sub>3</sub>) nanosheets were reported on BiSb alloy melt that presented a  $\alpha$ -Sb<sub>2</sub>O<sub>3</sub> dominated surface oxide layer.<sup>57</sup>

In addition, oxide layers can be collected *via* gas injection into LM melts in aqueous, organic or inorganic electrolyte solutions.<sup>50,58,59</sup> As examples, SnO nanosheets and SnO<sub>x</sub> nanoflakes were collected from Sn melt (>260 °C) and EBiSn melt (>139 °C), respectively.<sup>58,59</sup> The use of electrolyte solutions with various degree of acidity and alkalinity allow to gain access to the subsurface of the LM alloys and therefore collecting non-favorably formed 2D transition metal oxide nanosheets that would otherwise be covered by Ga<sub>2</sub>O<sub>3</sub>. Titanium dioxide (TiO<sub>2</sub>) and cobalt oxides (CoO<sub>x</sub>) nanosheets were formed from GaTi alloys and Ga-based alloys containing Co particles, respectively, using such method.<sup>60,61</sup> Other stamping, brushing, squeegeeing and high shear methods were devised for oxide skin collection from LM melts.<sup>62–68</sup>

The ultra-smooth and reactive surface of LMs can also be used for templating 2D materials. In contrast to solid metals, LMs possess a dynamic electrical double layer (EDL).<sup>26,69</sup> The physicochemical properties of the EDL of LMs can be manipulated with surface modifications, particle coatings and changes in the electrolyte interface.<sup>26</sup> Manganese dioxide (MnO<sub>2</sub>) and molybdenum sulfide (MoS<sub>2</sub>) monolayers were formed on the surface of EGaIn using galvanic replacement reactions between the surface of the LM and a permanganate (potassium permanganate) or molybdenum (ammonium tetrathiomolybdate) ionic source, respectively, in aqueous media.<sup>70,71</sup> Similarly, highly crystalline bismuth telluride (Bi<sub>2</sub>Te<sub>3</sub>) nanostructured platelets were synthesized at the surface of EGaIn drops.<sup>72</sup> As another example, the formation of layered double oxides was also achieved using a room temperature liquid alloy of Ga, In and Al.<sup>73</sup> In this study, the Al-containing LM alloy was placed in an

aqueous solution containing divalent cationic species including Ni<sup>2+</sup> or Co<sup>2+</sup> ions. Low-dimensional aluminum hydroxides formed spontaneously on the surface of the LM drop when immersed, and subsequently reacted with the cations present in solution. Following a hydrothermal process, the layered double oxides were formed.<sup>73</sup>

### 2.3 Nanopatterns from the solidification of LM surfaces

Solidification of post-transition LM systems can result in the formation of nanosized surface patterns and also phase separation during bulk solidification. Bulk phase separation during liquid to solid transition in molten metals is a well-known phenomenon of classical metallurgy.

The solidification and nanophase separation phenomena were investigated for the Bi–Ga system, including the dilute eutectic BiGa (Bi<sub>0.0022</sub>Ga<sub>0.9978</sub>) that resulted in Turing-like patterns when the surface was agitated and a solidification front was produced that propagated from the point of agitation.<sup>7</sup> During the solidification process, a Bi surface enrichment (up to 25 times) was reported to occur, which was associated with the formation of highly ordered Bi nanoscale patterns on the surface as presented in scanning electron microscopy (SEM) images and energy-dispersive X-ray spectroscopy (EDS) elemental mappings (Fig. 2a). The nanopatterns of Bi were reported at the subsurface of the solid alloy confined under the natural Ga oxide layer that protected them from oxidation. Similarly, nanopatterning was also found for other dilute binary and ternary Ga, Sn and Bi-based alloys.<sup>7</sup> In addition, post-transition/transition metal systems, such as Bi<sub>0.01</sub>Cu<sub>0.99</sub>, were also shown to present surface phase ordering at the sub-micron scale emerging during solidification.<sup>7</sup> The formation of surface nanopatterns was found to be dependent on multiple factors specific to each alloy including crystalline structures, solidification and oxidation thermodynamics. In another set of investigations, nanoscale patterns were observed on a Bi monolayer grown on niobium diselenide (NbSe<sub>2</sub>) that also resulted in Turing-like patterns (presented in Fig. 2b).<sup>15,74</sup>

In comparison, bulk solidification of post-transition metal alloys generally results in standard micron to sub-micron patterns of separated phases of fibrous, lamellar or rod shape structures. An example is presented for the solidification of BiSn alloys at the eutectic composition and also below and above the eutectic composition as presented in Fig. 2c. At the eutectic BiSn composition (57 wt% Bi), mostly fibrous structures were observed, which was attributed to solidification from the higher entropy system as opposed to non-eutectic ratios that solidified over a range of temperatures into more ordered lamellar and rod shape structures.<sup>23</sup>

### 2.4 Synthesis of nanoalloys and multi-elemental nanoparticles of post-transition LMs

By using LMs, nanoalloys and multi-elemental metallic nanoparticles can be synthesized based on a variety of metallurgical processes. In this regard, for synthesizing and designing nanoalloys and multi-elemental nanoparticles, synergistic physical and chemical properties between the added elements

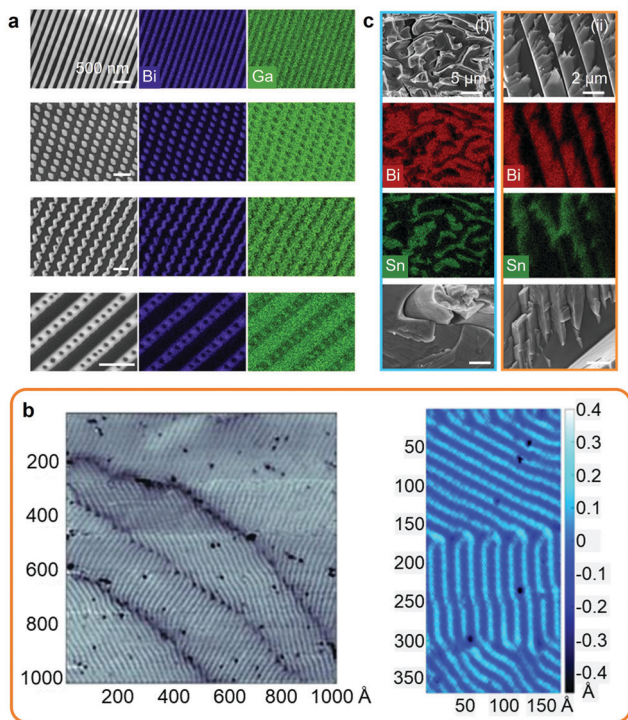


**Fig. 2** (a) SEM images and EDS mapping showing the surface nanoscale BiGa patterns including lamellae, rods, transitional and lamella-rod. Scale bars: 500 nm. Adapted with permission.<sup>7</sup> Copyright 2021, Springer Nature. (b) Surface topography of a single Bi monolayer grown on NbSe<sub>2</sub>. Adapted with permission.<sup>15</sup> Copyright 2018, AAAS. (c) SEM images and EDS mapping of the solidification patterns in the bulk of Bi<sub>0.4</sub>Sn<sub>0.6</sub> (i) and EBiSn (ii) alloys. Adapted with permission.<sup>23</sup> Copyright 2019, Springer Nature.

should be carefully considered.<sup>75</sup> In addition, strategies that have been used for the creation of ‘transition metal-based nanoalloys and nanoparticles’ can be adopted for post-transition metals.<sup>76</sup> During synthesis, considerations such as phase separation, formation of multiphase structures and multiple interfaces were reported to be thermodynamically driven, leading to the lowest energy of the system that determine the morphologies and crystal phases after solidification and phase separation.<sup>77</sup>

To date, multiple nanoalloy synthesis methods for creating ‘transition metal-based systems’ have been investigated including chemical reactions in aqueous or organic solutions combined with thermal reduction, microwave or laser irradiation, and sonochemistry.<sup>78</sup> Many of these methods rely on processes that incorporate precursors that are decomposed to establish nanoalloys. These growth processes generally require a combination of redox pathways, ligand assisted reactions and de-solvation steps. These steps can have a profound impact on crystal growth, directing the growth along certain crystal facets and impeding natural crystal expansion along others. In contrast, the synthesis of nanoalloys and nanostructured interfaces using ‘post-transition LM focused pathways’ have received less attention.<sup>7,23,28</sup>

**LM nanodroplets synthesis.** Room temperature liquid and low melting point post-transition metals and alloys can be dispersed and shaped into nanodroplets using a variety of

techniques. Top-down approaches have so far been the most popular techniques for the formation of such nanodroplets. They include mechanical agitation and sonication as illustrated in Fig. 1b.<sup>79</sup> Other mechanical synthesis and dispersion methods have also been reported including microfluidic, shearing, nebulization, extrusion and patterning of LMs.<sup>80–83</sup> Microfluidic approaches can produce more monodispersed yet relatively large micron-sized droplets (50 to 200 μm), while nebulization results in droplet dimensions below 200 nm with a narrow size distribution.<sup>80,81,84</sup> Shearing methods are particularly promising for the synthesis of micro to nano size droplet of LMs from low melting point alloys.<sup>82,85</sup> However to date, sonication methods based on probe sonicators and ultrasonic baths have remained the main techniques for synthesizing dispersions of LM micro and nanodroplets. Patterning and extrusion techniques have also been used for the formation of LM drops, some of which offer narrow size distributions; however, the obtainable LM droplet dimensions generally remain in the microscale ranges.<sup>83,86,87</sup>

Post-transition LMs such as EGaIn and Galinstan have been routinely processed into nanoscale entities using sonication techniques. The sonication temperature, choice of the solvent, pH conditions and addition of stabilizer molecules were reported to drastically influence the resulting dimensions of the nanodroplets and of materials which are co-produced in the process.<sup>79</sup> Without the usage of surfactants, sonication of liquid Ga and its alloys generally result in the formation of droplets that are covered with Ga<sub>2</sub>O<sub>3</sub> or monohydroxide (GaOOH) coatings, depending on the surrounding solvent. However, with excess sonication time (usually more than 20 minutes), these liquid Ga and its alloys may totally transform into Ga<sub>2</sub>O<sub>3</sub> and GaOOH nanoflakes, nanoplate or nanorod crystals.<sup>88–90</sup> The transformation is due to the heat generated by the sonicator rather than sonochemistry.<sup>89</sup> On another note, Ga itself has appeared to be a catalytic material that can break strong covalent bonds during sonication even those of stable molecules such as N<sub>2</sub>.<sup>91</sup> In this regard, nitridation of Ga-based alloys has been reported *via* sonication in the presence of nitrogen-rich precursors such as N<sub>2</sub> gas or polyvinylpyrrolidone (PVP) surfactant resulting in the formation of mixed gallium nitride (GaN) and GaOOH nanocrystallites.<sup>91</sup>

Besides the sonication duration and power intensity, other factors such as temperature and the presence of charged molecules or surfactants were reported to induce shape transformation of LM nanodroplets. For example, dealloying phenomena were shown to occur in Ga-based nanodroplets *via* moderate heating either during or after sonication or *via* sonication in alkaline solution.<sup>89,97</sup> EGaIn nanospheres were observed to transform into individual GaOOH nanorods together with solid In nanoparticles by heating the solution to 70 °C. In this case, the heating could drive the transformation of EGaIn nanodroplets from liquid to solid *via* selective dealloying of Ga through its oxidation into GaOOH nanorods. Interestingly, the use of surfactants was shown to prevent dealloying during heat treatment.<sup>89</sup>

A drawback of sonication is the broad particle size distribution of the produced nanodroplets. To minimize the size

Table 2 Post-transition LM nanodroplets synthesis techniques

Synthesis technique	Ga-based LM droplets size range	<i>In situ</i> functionalization	Applicability to other low-melting point metals and alloys
Sonication <sup>81,92–96</sup>	<10 nm, <sup>a</sup> 50 to 1000 nm	Yes	Yes
Shearing <sup>82,85</sup>	~10 nm and below 10 μm	Yes	Yes
Microfluidic <sup>80,84,93</sup>	50 to 1000 nm, <sup>b</sup> 50 to 200 μm	Yes	Not reported
Patterning <sup>83</sup>	50 to 500 μm and more	Not reported	Not reported
Extrusion <sup>40,87</sup>	10 to 500 μm and more	Not reported	Not reported

<sup>a</sup> Sonication coupled with laser irradiation. <sup>b</sup> Microfluidic coupled with sonication.

distribution of the nanodroplets, different strategies, such as combined on-chip sonication, dynamic temperature control and centrifugation were proposed.<sup>92,93</sup> Other techniques, such as coupling laser irradiation and sonication approaches, were also reported that resulted in remarkable size reduction of droplets to below 10 nm.<sup>94,95</sup> A brief description of the different nanodroplet preparation techniques is presented in Table 2.

**LM nanodroplets functionalization.** LM nanodroplets can be functionalized *in situ* during sonication using a variety of molecules to prevent their nucleation, control their particle size distribution or promote their colloidal stability.<sup>96,98</sup> LM nanodroplets can be functionalized during their synthesis *via* direct grafting of organic materials on their bare reactive surface or *via* anchoring of molecules on the hydroxyl groups present on the oxide layer.<sup>79</sup> Functionalization of LM nanodroplets was reported through a range of molecules bearing functional anchoring groups such as silane, amine, thiol, catechol, phosphate, trithiocarbonate, and other acidic groups.<sup>46,81,93,96,99–105</sup> As an example, diblock copolymers with short poly(acrylic acid) anchoring segments were attached to the Ga oxide skin of EGaIn nanodroplets to form polymer brushes.<sup>106</sup> These polymer brushes/EGaIn nanodroplets exhibited good re-dispersibility with narrow size distribution in a variety of solvents. The surfactants and organic materials that are incorporated on the surface of LM droplets can have significant effect on the properties of the nanodroplets, granting them specific bio-functionalities, especially in biotechnology and nanomedicine applications.<sup>3,107</sup> Such coatings can also improve the stability of suspensions of these nanodroplets. It has been reported that grafting of a hydrophobic polymer layer comprising of poly(1-octadecene-*alt*-maleic anhydride) on the surface of LM nanodroplets enabled them to remain stable for more than 60 days in a buffer solution without oxidation-induced aggregation.<sup>105</sup> Altogether, functionalization of LM nanodroplets present great opportunities for tuning their properties for various applications.

**Heterogeneous nanostructures formation.** Post-transition LM alloys provide the possibility of creating a range of interfacial heterostructures *via* controlling the alloy composition and alteration of the ambient conditions.<sup>8,90</sup> Heterogeneous multiphase LMs were reported in supersaturated states, when a solute element, above its maximum solubility, is added into a LM as the solvent.<sup>8,108</sup> The concentration limit at which the LM alloy remains liquid is specified by the relevant phase diagrams.<sup>109</sup> Although, it should be considered that observations might significantly diverge from classical phase diagrams

when the dimensions of droplets becomes smaller. Additionally, LM nanodroplets can exhibit homogeneous or heterogeneous cores and surfaces of various compounds, depending on how they were designed and synthesized. Supersaturation and then cooling can produce secondary solid phases in the LM pool. As an example, cerium (Ce) crystals were synthesized inside liquid Ga or Galinstan droplets using this method.<sup>8</sup> Below the Ce solubility limit, the LM alloy presented a homogeneous core matrix and atomically smooth surface, while above the Ce solubility limit, self-forming solid Ce nanoparticles emerged encapsulated within the liquid Ga-based core matrix.<sup>8</sup>

Information from phase diagrams can be used for the creation of interesting solid-liquid nanoparticles. For instance, intermetallic compounds can be formed, based on phase diagrams, by bringing a secondary metal into intimate contact with LMs. This method can be used with metals that are not soluble in the LM of interest, such as nickel (Ni), molybdenum (Mo) and copper (Cu) in LM Ga. As an example, it was demonstrated that by dispersing solid Cu particles in Ga-based LMs, intermetallic Cu<sub>2</sub>Ga crystals were produced.<sup>110,111</sup> Interestingly, the Cu<sub>2</sub>Ga crystals were seen to diffuse into the LM matrix in time.<sup>110</sup> The formation of Cu<sub>2</sub>Ga intermetallic was also reported in Galinstan sandwiched between two Cu current collectors and upon applying a high DC current.<sup>112</sup>

**Solidification of LM nanodroplets.** Sonication of LM melts to form particles combined with subsequent solidification offers unique opportunities for synthesizing solid nanoparticles of post-transition metals and the observation of phenomenon such as supercooling (*i.e.* materials that remain liquid below their melting point). These processes allow to study surface physicochemistry, oxide formation mechanisms and catalytic microkinetics occurring at the dynamic surface of LM nanodroplets. Significantly, the formation of LM nanodroplets and their subsequent solidification, can also lead to altered thermodynamics with perturbed core and interfacial chemistries at the nanoscale, as compared to bulk LM melts.

An interesting co-existence of liquid and solid phases has been reported below the melting point of post-transition metals. Such examples were demonstrated with the simultaneous existence of solid Ga crystals within liquid Ga encapsulations at the nanoscale.<sup>1</sup> It has been suggested that the reactivity of the support utilized during the deposition of the Ga nanodroplets played a crucial role in the nucleation of the solid Ga phase within the Ga liquid. In this case, Ga nanodroplets deposited on sapphire (c-Al<sub>2</sub>O<sub>3</sub>) produced solid Ga nanoparticles within the liquid encapsulation.<sup>1</sup> However, on amorphous

glass substrates, only a Ga liquid phase was observed, which was ascribed to the weaker wetting of liquid Ga on glass in comparison to sapphire and also to the high activation energy of Ga diffusion into the glass. On more reactive substrates, such as silicon (Si), Ga dissolves into the Si matrix forming an interfacial layer of gallium silicide.<sup>1</sup> The solid Ga particles and encapsulating liquid Ga nanodroplets formed on the different substrates are shown in Fig. 3a as characterized using high angle annular dark field scanning transmission electron microscopy (HAADF-STEM) and EDS mapping.<sup>1</sup>

In another interesting observation, controlled phase transitions in homogeneous binary EGaIn nanodroplets were demonstrated *via* thermal cycling.<sup>14</sup> Multiple phase transitions were observed, from an In solid core in a Ga liquid shell to a Janus type material with both solid In and Ga phase separated as presented in Fig. 3b. This phenomenon was also shown in ternary Ga–In–Sn alloys with the formation of a solid bi-crystal cores of In and Sn in solid Ga shells, which indicated the importance of the concentration of the minority element in the Ga liquid base for the formation of specific liquid/solid nanostructures.<sup>14</sup> In addition, supercooling was reported to be exacerbated by the size reduction of bulk LM to micro and nanodroplets.<sup>113,114</sup>

Taking advantage of the solidification of LM nanodroplets of post-transition metals also provide great opportunities for creating solid metal and metal oxide nanoparticles. For synthesizing nanodroplets of post-transition metals and alloys of higher melting point than Ga, sonication or shearing processes can be conducted in appropriate high boiling point solutions. The sonication of molten Sn, Bi and their alloys (eutectic and

non-eutectic) was reported in silicone oil, which has a boiling point above the respective melting points of each of the metals.<sup>23</sup> In this case, Bi and Sn nanoparticles were formed with sizes below 200 nm. When the eutectic BiSn alloy was used, the synthesized nanoparticles showed intricate structures of BiSn metallic core, multiple shells of Sn oxides (SnO and SnO<sub>2</sub>) and a surface oxide shell of mixed SnO and bismuth oxide (Bi<sub>2</sub>O<sub>3</sub>), as represented in Fig. 3c.<sup>23</sup> In this example, the eutectic BiSn nanoalloys showed more lines and surface defects, edge dislocations and increased boundaries in comparison to other BiSn nanoalloys.<sup>23</sup> Additionally, this study revealed that agitation resulted in the formation of more diverse surface oxides on nanodroplets rather than simply SnO present on the surface of bulk of BiSn alloys due to the change of the thermodynamic conditions.

The formation of eutectic BiSn microparticles with nano-sized separated domains of Bi and Sn is presented in Fig. 3d.<sup>23,28</sup> Furthermore, the addition of 2 wt% In into the eutectic BiSn alloy (Bi<sub>56</sub>Sn<sub>42</sub>In<sub>2</sub> alloy) was reported to dramatically decrease the particles size distribution during sonication, which presented perfect separation of the Sn and Bi domains and In coating (Fig. 3d).<sup>28</sup>

In another example, low-melting point ternary nanoalloys were formed *via* sonication in glycerol or DI water.<sup>19,115</sup> Here, Field's metal melt was processed into nanoparticles with an average size of 250 nm. The synthesized nanoparticles presented spherical core/shell metal/metal oxide heterostructures including In(OH)<sub>3</sub> oxide phase, binary BiIn<sub>2</sub> and Sn<sub>0.8</sub>In<sub>0.2</sub> metallic phases after solidification, which indicated phase separation during the solidification of the liquid alloy.<sup>115</sup>

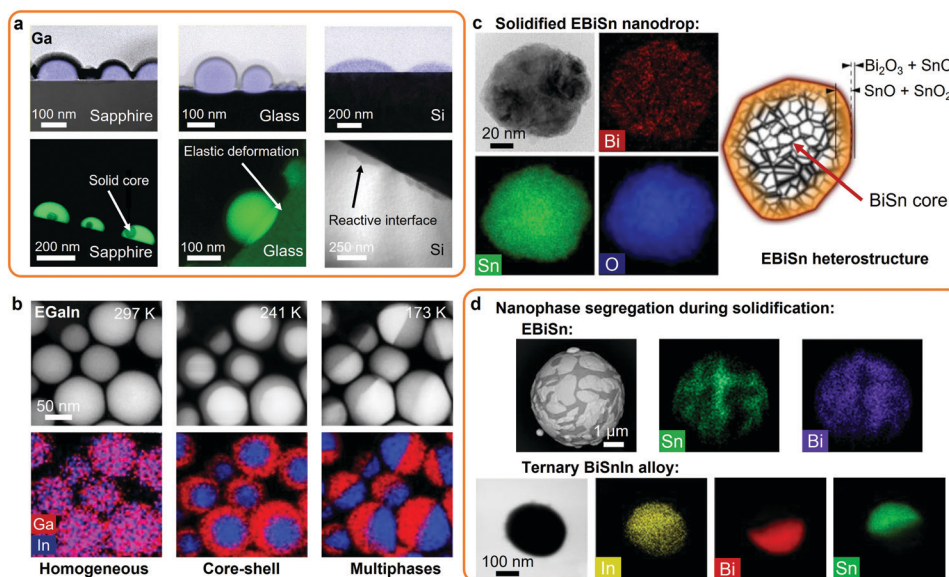


Fig. 3 (a) Solid core liquid shell Ga nanodroplets formed on crystalline, amorphous or reactive substrates (HAADF-STEM images and Ga EDS mapping). Adapted with permission.<sup>1</sup> Copyright 2016, Springer Nature. (b) Homogeneous and heterogeneous EGaIn nanodroplets formed *via* thermal cycling (HAADF-STEM images and EDS mapping). Adapted with permission.<sup>14</sup> Copyright 2019, Elsevier. (c) Solidified EBiSn nanodrop presenting a metal core and a complex oxide shell structure (TEM image and EDS mapping). Adapted with permission.<sup>23</sup> Copyright 2019, Springer Nature. (d) Nanophase distribution across EBiSn (SEM image and EDS mapping) and ternary BiSnIn alloys (TEM image and EDS mapping). Adapted with permission.<sup>28</sup> Copyright 2020, ACS Publications.



The principles of nanometallurgy applied to post-transition-based liquid and alloys is only beginning to be realized for the formation of nanoalloys. Sonication and solidification of low melting point alloys provide new routes for the creation of functional micro and nano features and chemistries that are otherwise not accessible in bulk LM melts. While some valuable effects of nano-ordering phenomena in the core and at the interfacial oxide layer have been observed in single and multi-elemental LMs, the realization of many more possibilities remains to be achieved.

### 3. Nanocomposites based on LMs

In this section, the possibility of creating composites, with nanostructured fillers, using LMs are presented. The LM nanocomposites that are discussed here can be made of nanosized LMs dispersed into polymeric materials, grafted with polymeric networks, or made of nanodimensional inorganic solid particles dispersed into a LM phase. The composites can be made in liquid, solid, or heterogeneous states and formed into matrices such as elastomers, hydrogels, foams and semisolids.

#### 3.1 LM polymer and organic material nanocomposites

In the previous sections, we described how LM nanodroplets can be synthesized. These nanodroplets can then be encased into polymers to form LM polymer nanocomposites with several useful properties. Their formation is often reported to follow a one-pot mixing method with direct synthesis of the LM nanodroplets into a pre-polymeric liquid before casting and curing.

LM polymer nanocomposites based on non-conductive matrices present high initial electrical resistivity ( $> \text{k}\Omega \text{ m}$ ), even with a high-volume fraction of LM nanodroplets ( $\phi \geq 50\%$ ) due to the presence of a naturally insulating surface oxide layer on the LMs and a thin layer of polymer that separates the LM nanodroplets.<sup>20,116–121</sup> The composite can be rendered conductive by a mechanical compression step that ruptures the oxide layer and/or polymer coating, and merges the LM nanodroplets.<sup>20,119,120</sup> Laser irradiation, or any other heat sources, can also achieve electrical percolation by merging the LM droplets *via* thermal expansion.<sup>122,123</sup> To partially prevent the oxidation of the LM nanodroplets, they can be synthesized *ex situ* in a solvent containing a trace amount of an acidic or basic mediator.<sup>119,122</sup> Co-fillers can also be mixed together with the LM nanodroplets to simultaneously provide enhanced conductivity as well as new properties to the nanocomposites.<sup>16,119,124</sup> In one example, the addition of graphene flakes was shown to augment both the electrical conductivity and increase the mechanical integrity of the matrix.<sup>119</sup> In another example, the formation of anisotropic LM-based nanocomposite with enhanced conductivity was reported *via* the magnetic alignment of solid magnetic co-fillers before curing of the elastomer matrix.<sup>124</sup>

Polymers with specific functional groups can be used for dispersing and stabilizing the nanodroplets resulting in electrically

conductive LM composites without the need for mechanical activation. Such examples are seen for LM hydrogel composites which provide ionic conductive coatings.<sup>47,125–129</sup> In addition when hydrated, the hydrogel matrix and LM phase demonstrate flexibility, stretchability and self-healing properties. As an example, EGaIn nanodroplets with an average size of 220 nm, were synthesized *in situ* in an aqueous poly(vinyl alcohol) (PVA) solution prior to cross-linking.<sup>47</sup> Other hydrogels with distinct responsive properties remain to be investigated as functional matrices for the synthesis of LM nanocomposites.<sup>130</sup>

The co-addition of functional molecules, such as thermochromic pigments, in the elastomer matrix was also reported. In such case, Joule heating of the LM phase induced a color change across the LM composite.<sup>131</sup> A wide range of functional molecules as co-additives in LM composites and nanocomposites systems remain to be studied.<sup>132</sup>

Organic materials can be reacted on the surface of LM nanodroplets, during or after their synthesis, to form LM organic networks. During their synthesis, the reactive surfaces of the nanodroplets can be manipulated resulting in the grafting and polymerization of organic compounds. The *in situ* formation of LM nanodroplets was reported to directly initiate the polymerization of various monomers.<sup>5,133–135</sup> As an example, the synthesis of EGaIn nanodroplets *via* sonication was shown to initiate free radical polymerization reaction of vinyl monomers in an aqueous solution (Fig. 4a).<sup>5</sup> Alternatively, LM nanodroplets can be dispersed into a monomeric solution before the polymerization reaction and utilized as nucleation sites. For example, polyaniline (PANI) nanofibers were synthesized at the surface of EGaIn nanodrops leading to EGaIn/PANI nanocomposites as characterized with SEM and transmission electron microscopy (TEM) (Fig. 4b).<sup>18</sup> In another example, the oxide layer on the surface of EGaIn nanodroplets was covalently functionalized with poly(methyl methacrylate) (PMMA).<sup>24</sup> The TEM images of the PMMA-grafted EGaIn nanodroplets are presented in Fig. 4c along with the resulting EGaIn/PMMA composite, which was compared to a EGaIn/PDMS composite prepared by mechanical dispersion. Similarly, *in situ* polymerization of EGaIn/lactones nanocomposites were reported.<sup>134</sup> Such approaches may lead to more homogeneity across the composite as compared to mechanical mixing.<sup>24</sup> In a different approach, EGaIn droplets functionalized with acrylate ligands were cross-linked into a LM organic network with a high weight fraction of LM ( $> 99.9 \text{ wt}\%$ ), which presented stretchability and electrical conductivity under strain as shown in Fig. 4d.<sup>27</sup>

#### 3.2 LM inorganic nanocomposites

Inorganic materials can also be mixed with nanosized or bulk LMs to form LM inorganic nanocomposites. The LM phase can offer distinct advantages in comparison to conventional media including an oxygen free environment, high thermal and electrical conductivities, and high catalytic activity. These characteristics provide both opportunities and challenges for establishing inorganic nanocomposites with LMs.

LM nanodroplets can be modified during its synthesis for the formation of inorganic nanocomposites. As an example,

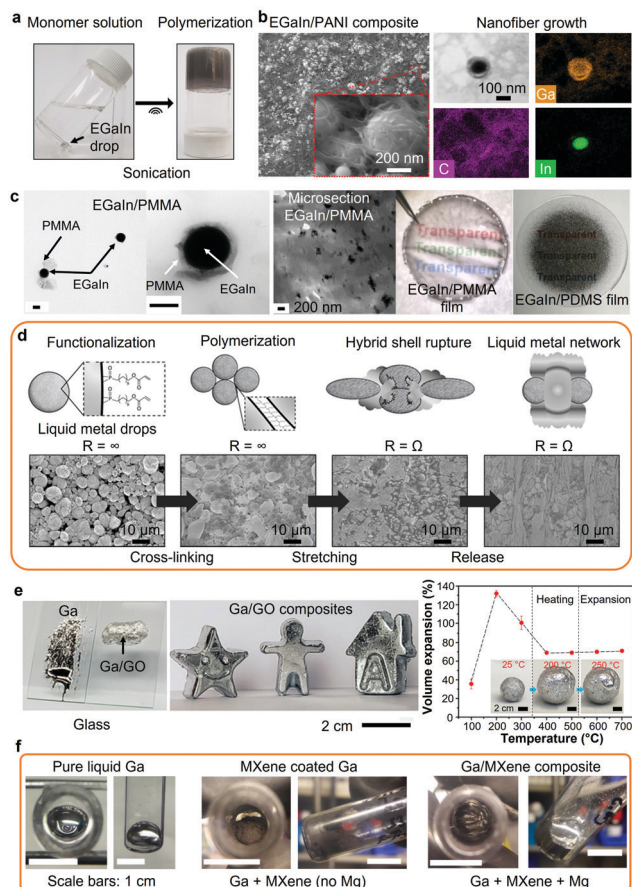


**Fig. 4** (a) EGaIn-initiated free radical polymerization reaction of a vinyl-based monomer. Adapted with permission.<sup>5</sup> Copyright 2019, ACS Publications. (b) EGaIn/PANI nanocomposite with EGaIn nanodroplets integrated into the PANI nanofiber network (SEM images and TEM/EDS mapping). Adapted with permission.<sup>18</sup> Copyright 2020, ACS Publications. (c) TEM images of the PMMA-grafted EGaIn nanodroplets and photographs of the resulting EGaIn/PMMA nanocomposite and compared to a EGaIn/PDMS nanocomposite prepared by mechanical dispersion. Adapted with permission.<sup>24</sup> Copyright 2019, Springer Nature. (d) Polymerization of functionalized EGaIn nanodroplets forming a LM network and subsequent mechanical activation with associated SEM images. Adapted with permission.<sup>27</sup> Copyright 2019, Wiley-VCH. (e) Photographs of liquid Ga and Ga/GO putty on glass, examples of shaped Ga/GO putties and volume expansion of the Ga/GO putty as a function of temperature with optical photos showing the expanded putties. Adapted with permission.<sup>29</sup> Copyright 2021, AAAS. (f) Photographs of the top and side of Ga/MXene composite after ultrasonic agitation with or without addition of Mg. Adapted with permission.<sup>31</sup> Copyright 2019, ACS Publications.

Galinstan micro and nano droplets with solid silver (Ag) and gold (Au) inclusions were synthesized during sonication of Galinstan in AgNO<sub>3</sub> and KAuBr<sub>4</sub> solutions, respectively.<sup>136</sup> In another example, micro and nanodroplets of Galinstan were utilized as surface templates for the formation of copper species including CuO, Cu<sub>2</sub>O and Cu *via* galvanic replacement using CuSO<sub>4</sub> as the precursor.<sup>137</sup> The crystals stoichiometry and growth could be controlled by adjusting the pH and reaction time. In a similar approach, EGaIn and manganese dioxide core/shell nanostructures were synthesized *via* sonication using KMnO<sub>4</sub> as the Mn source.<sup>70</sup> Co-sonication of EGaIn and 2D

tungsten oxide (WO<sub>3</sub>) flakes was also performed for synthesizing EGaIn/WO<sub>3</sub> nanocomposites.<sup>138</sup> The presence of WO<sub>3</sub> flakes during sonication also increased the shearing forces resulting in EGaIn droplets with reduced sizes. Furthermore, EGaIn micro and nanodroplets were encapsulated by 2D graphene materials including GO, reduced GO (rGO) and functionalized GO post-synthesis or during synthesis.<sup>139,140</sup> In such cases, sonication of EGaIn in a GO solution resulted in EGaIn nanodroplets encapsulated with rGO and the reduction of the GO flakes were taking place at the same time.<sup>139</sup> Encapsulation of EGaIn nanodroplets with metal-organic frameworks (MOFs), such as ZIF-8, was also reported.<sup>141</sup>

The surface of LM droplets can be functionalized with micro and nanoparticles of metals, metal oxides, carbon-based and also with some organic materials, resulting in the formation of the so called 'LM marbles'.<sup>26,69,142,143</sup> LM marbles are typically synthesized by rolling a LM droplet on a bed of particles or by immersion in a colloidal suspension.<sup>26</sup> The particles then adhere to the LM surface. LM marbles were coated with semiconductor particles, such as ZnO and WO<sub>3</sub>, insulators, such as Teflon and SiO<sub>2</sub>, and also with carbon nanotubes.<sup>26,69,142,143</sup>

Bulk LMs can be utilized for the dispersion of inorganic particles forming LM inorganic nanocomposites with enhanced mechanical strength and/or thermal properties, and also with other functionalities such as the modulation of supercooling.<sup>29,144-146</sup> In such cases, strong shear forces should be applied to assist in wrapping the incorporated particles into the LM bulk. To date, Ga and Ga-based inorganic nanocomposites have been synthesized with 2D transition-metal carbides and nitrides (MXenes), functionalized carbon nanotubes, graphene, graphene oxide, graphite, diamond, tungsten and silicon carbide for a variety of applications.<sup>29,31,144,147,148</sup> Similar to any other liquid media, mixing of particles in LMs requires interfacial and dimensional compatibility.<sup>29</sup> As an example, large GO flakes (>10 μm) were dispersed in Ga-based LMs forming stable inorganic nanocomposites that could be shaped into various forms as shown in Fig. 4e.<sup>29</sup> Furthermore, thermal post-treatment of Ga/GO LM nanocomposites allowed for the formation of Ga-based foams. Elemental addition, such as Mg in Ga-based LMs, was also reported to facilitate the binding and wetting of MXenes at the LM interface (Fig. 4f).<sup>31</sup>

## 4. Emerging applications of nanostructured LMs

In this section, the use of nanostructured LMs in different emerging applications are presented. The main subsections are dedicated to the most researched applications including soft electronics, sensors, catalysis, energy, nanomedicine and biomedical applications, while a final subsection is presented for other applications.

### 4.1 LM soft electronics

Soft electronics is an emerging class of electronics able to operate under mechanical deformation, which are critical for

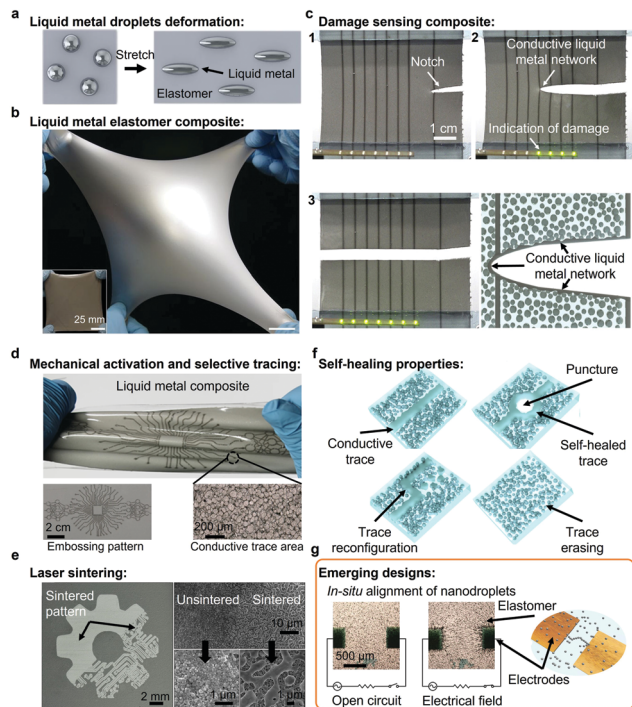


**Fig. 5** (a) Schematic illustration of the deformation of LM droplets in the direction of the stretching. (b) Stretchable LM elastomer composite. Adapted with permission.<sup>2</sup> Copyright 2017, National Academy of Sciences. (c) Propagation of a cut in a LM composite and formation of conductive LM network indicating of the damage. Adapted with permission.<sup>9</sup> Copyright 2019, Wiley-VCH. (d) Intricate embossing pattern of electrically conductive LM traces in an elastomer-based composite. Adapted with permission.<sup>20</sup> Copyright 2018, Springer Nature. (e) Electrically conductive LM trace formed via laser sintering on an elastomer matrix (SEM images). Adapted with permission.<sup>25</sup> Copyright 2018, ACS Publications. (f) Illustration of the self-healing properties of a LM elastomer nanocomposite. Adapted with permission.<sup>30</sup> Copyright 2021, Springer Nature. (g) Dielectrophoretic process for *in situ* alignment of LM nanodroplets in an elastomer matrix. Adapted with permission.<sup>33</sup> Copyright 2020, Wiley-VCH.

the formation of soft junctions, artificial skins, soft robotics and wearable electronics. Unlike rigid electronic materials, such as Au and Cu, LMs are intrinsically stretchable with mechanical properties close to other liquids. LMs and LM nanodroplets present fluidity and deformability; bulk LMs flow readily like water, although the presence of solid surface species (*e.g.* oxides) complicates the rheological behavior, but also offers opportunities for shaping the metal. All those properties are particularly valuable characteristics for the formation of soft electronics.<sup>2,20,118,119,149–151</sup> During stretching and deformation, LM and LM nanodroplets can deform in the direction of the applied strain, in contrast to solids, as illustrated in Fig. 5a.<sup>2,9</sup>

The very high surface tensions of LMs ( $\sim 724 \text{ nN m}^{-1}$  for bare Ga and  $\sim 624 \text{ nN m}^{-1}$  for bare EGaIn<sup>152,153</sup>) represent an important challenge for the formation of stable non-spherical shapes, such as wires and sharp features, at the nanoscale. LM wires formed by 3D printing remain in the micro range ( $\sim 2 \mu\text{m}$  in width), while the direct patterning of LMs can, in theory, achieve sub-micron resolution.<sup>154,155</sup> To date,

sub-micron scale EGaIn patterns were achieved with features as small as  $\sim 180 \text{ nm}$  using a hybrid electron-beam and soft lithography method.<sup>156</sup> In comparison, sub 10 nm LM nanodroplets have been reported using mechanical agitation methods.<sup>82,94</sup>

LM probes can be employed as soft junctions and for surface electrical characterization.<sup>26,157,158</sup> As examples, LM marbles coated with semiconducting particles were utilized for the formation of soft contacts with LM–semiconductor junctions.<sup>26</sup> LM nanotips, with sharp apices between 10 and 100 nm, shaped by pulling (tensile forces) a drop of LM, can be used as soft electronic contacts to surfaces.<sup>157</sup>

Biphasic liquid/solid LM nanocomposites can be synthesized with the addition of secondary materials, such as Cu, Ag, Ni particles or CNTs, as previously mentioned, and can present enhanced electrical and thermal conductivities, and also altered rheological characteristics as compared to the plain LM phase. Biphasic LM nanocomposites were extruded, printed or painted on substrates forming electronic components and soft contacts.<sup>110,144,147,159–162</sup> As an example, LM/CNTs nanocomposite was 3D printed into soft electrically conductive wires (5  $\mu\text{m}$  in diameter) with 3D interconnections that were made possible by the enhanced stability of the printed patterns with the LM/CNTs nanocomposite as compared to plain LM.<sup>144</sup>

LM nanodroplet inks and slurries can be directly utilized for the writing or printing of soft electronic patterns on flexible substrates.<sup>163–166</sup> A mechanical activation step is required as the polymer coating or oxide layer on the LM nanodroplets is electrically insulating and makes the printed pattern non-conductive. Alternatively, spraying process of LM can generate sufficient kinetic energy to merge the LM droplets on impact producing conductive paths.<sup>167</sup>

The insulating nature of the LM nanodroplets can constitute an advantage for soft electronic device fabrication. As an example, the selective mechanical merging of LM nanodroplets allows for the formation of tunable antennas for wireless communication.<sup>150</sup> In this work, the operating frequency of the antenna was tuned by controlling the merging length across of EGaIn slurry injected into microchannels. Biphasic liquid/solid conductive traces can also be formed from the thermal treatment of a sprayed EGaIn nanodroplets slurry.<sup>168</sup> The resulting traces presented a LM phase contained by a crystalline solid top layer, which provided an enhanced interface with the formed solid particles as compared to biphasic LM inorganic nanocomposites.

EGaIn and Galinstan nanodroplets were also proposed as electron transport materials and self-healing metal contacts in perovskite, flexible perovskite and organic solar cells.<sup>94,95,169,170</sup> As an example, LM nanodroplets were shown to facilitate the electron-transfer process and also provide temporary electron storage at the grain boundaries of perovskite materials.<sup>94</sup>

LM inks are typically based on LM nanodroplets functionalized with a range of polymeric compounds, such as polysaccharides or tannic acid, that provide adhesion properties to the LM inks.<sup>46,171</sup> In one example, coils and electrode arrays were fabricated by inkjet printing of a Galinstan nanodroplets

dispersion on flexible PDMS substrates.<sup>166</sup> Additionally, complex conductive patterns could be drawn using ballpoint systems. LM patterns were also formed *via* maskless UV photolithography process using a EGaIn/photoresist nanodispersion.<sup>172</sup> The EGaIn/photoresist patterns were then mechanically activated to produce conductive traces with a resolution of 10  $\mu\text{m}$ , which included sharp features.

Highly stretchable LM polymer nanocomposites that maintain conductivity up to 1200% strain were reported.<sup>2,6,30,121</sup> An example of a LM polymer soft composite system is presented in Fig. 5b.<sup>9</sup> As previously mentioned, mechanical activation of LM polymer nanocomposites is required to form electrically conductive materials. Mechanical activation can be non-selective across the whole material or selective for the formation of functional conductive LM traces. As an example, an array of conductive traces on a soft elastomer was demonstrated as sensors of mechanical damage (Fig. 5c).<sup>9</sup> An innovative strategy to form complex soft electronic circuits is based on embossing techniques, where a specific pattern is pressed on the material. Elaborate embossed LM patterns were formed with metallic conductivity (Fig. 5d).<sup>20,30</sup> Complex patterns can also be formed using direct laser writing (Fig. 5e).<sup>122,123</sup> In specific cases, the mechanical patterning and activation process can be reversed while the traces can be reconfigured using chemical treatments.<sup>30</sup> In addition, LM traces formed on hydrogel-based soft electronics can be formed in the dry state and then erased with hydration of the hydrogel.<sup>127</sup>

LM traces formed from merging LM nanodroplets exhibit self-healing properties. In an early study, encapsulated EGaIn microdroplets ( $\sim 3 \mu\text{m}$ ) into a urea-formaldehyde resin acted as a healing agent restoring the conductivity of the gold circuitry upon mechanical fracture.<sup>173</sup> Similarly, the self-healing properties of LM traces were shown within elastomers with reconfiguration of the LM conductive pathways across cutting, tearing and puncture damage as illustrated in Fig. 5f.<sup>20,30</sup> Functionalized LM nanodroplets can also provide self-healing properties to the base polymer material.<sup>174</sup> Additionally, LM soft

electronics present exceptional resistance to crack and tear propagation due to the deformable nature of the LM additives, which can redirect stress away from the crack.<sup>175</sup>

LM soft electronics with reversible insulating and conductor behavior were also synthesized.<sup>121,176</sup> As an example, a LM soft electronic circuit containing EGaIn droplets showed insulating behavior above the melting point of the alloy and conducting behavior during the freezing cycle due to the expansion of the Ga droplets creating a conductive percolation path across the insulating polymeric matrix.<sup>121</sup> The recyclability of LM-based soft electronics is also emerging *via* the dissolution of the polymer matrix and separation of the LM phase under mechanical agitation.<sup>30,176</sup> However, the formation of conductors from LM nanodroplets usually requires a high loading of nanodroplets to achieve percolation. To reduce the loading of LMs, the alignment and sintering of EGaIn LM nanodroplets into liquid microwires was demonstrated by dielectrophoresis in a stretchable silicone matrix before curing (Fig. 5g).<sup>33</sup> These particle-based inks can also be used as self-healing inks that can be assembled *in situ* to repair broken electrical pathways.

## 4.2 Sensors

Nanosized LMs present great opportunities as sensing materials due to their variable electrical resistance under mechanical deformation, tunable semiconducting oxide layer, ease of synthesis and unique interaction phenomena with heavy metal ions. Nanostructured LMs and nanocomposites were utilized as pressure and motion sensors, for the sensing of electromagnetic fields, gases and vapors, heavy metal ions, and also utilized as plasmonic-based sensors (Table 3). In addition, nanostructured LMs present great opportunities for biomedical imaging and biosensing.

**Pressure and motion sensors.** Soft and deformable LM micro and nanocomposites present variable electrical conductivities under various mechanical deformation processes, such as stretching, pressing and twisting. In contrast to most composites integrating solid conductive fillers, LM-based composites exhibit

**Table 3** Sensing applications of LMs and LM composites

Sensor type	LM	Media	Ref.
Pressure and motion	EGaIn EGaIn/graphene Galinstan EGaIn/Ni Ga/rGO	Elastomer, hydrogel, polymeric foam	6, 20, 46, 119, 128, 165, 178 and 182
Electromagnetic	EGaIn and Fe	Elastomer	16
Gases and vapors	Oxidized Galinstan Oxidized GaIn, GaSn and GaZn EGaIn/WO <sub>3</sub> EGaIn/PANI EGaIn-Based/polydopamine	Selected gases (H <sub>2</sub> , NO <sub>2</sub> , H <sub>2</sub> S, NH <sub>3</sub> , CH <sub>4</sub> , acidic vapors)	18, 22, 100, 138 and 192
Heavy metal ions	Galinstan(bulk)/WO <sub>3</sub> (nano) Galinstan(nano)/WO <sub>3</sub> (nano) EGaIn/tannic acid EGaIn/rGO	Electrolyte (Pb <sup>2+</sup> , Cd <sup>2+</sup> )	26, 46, 139 and 197
Plasmonic-based	Ga EGaIn GaN/GaOOH BiGa and AgGa nanopatterns	Substrate supported, suspension	7, 91, 198 and 201–203

positive piezoconductivity, which corresponds to an increase of conductivity upon strain.<sup>16,124,177</sup> These changes in electrical properties under mechanical loads are particularly useful for the formation of pressure and motion sensing LM/polymer composites.<sup>20,119,149</sup> Porous foam-like LM nanocomposites can also be prepared, which showed increased electrical conductivity when pressed.<sup>178</sup> Additionally, a LM-based elastomer foam integrating micron-sized LM droplets and presenting positive piezopermittivity was utilized as pressure and touch sensor based on the change of capacitance across the material under various deformations.<sup>179</sup> In addition, glues incorporating Galinstan nanodroplets were reported for pressure sensitive connections.<sup>180</sup> Other LM-based materials, such as LM hydrogel nanocomposites and microscale LM printing on stretchable substrates, were incorporated in strain sensors.<sup>128,165</sup> Furthermore, LM-based nanocomposites with advanced designs can be employed as strain sensors with the ability to record motions when integrated with different objects and wearables such as gloves (Fig. 6a).<sup>6,179</sup>

**Electromagnetic sensing.** LMs were shown to react to magnetic field stimulation and also present magnetocaloric properties.<sup>181</sup> The magnetic properties of LMs can be significantly altered with the dispersion of magnetic micro and nanoparticles into or with LMs forming composite materials with high electrical conductivity and, at the same time, magnetic sensitivity.<sup>108,124,142,182–185</sup> Magnetic LM-based elastomer micro and nanocomposites were also synthesized.<sup>16,47,186</sup> As an example, EGaIn was dispersed along with micro Fe or Ni particles in a PDMS matrix forming magnetic stretchable conductors, which were demonstrated as magnetic field sensors.<sup>16</sup> Responses of the magnetic LM-based material to a magnetic field and its structure are shown in Fig. 6b. In this example, changes in electrical resistance were attributed to the alignment of the magnetic particles in the direction of the magnetic field and to the mechanical deformation of the micro/nanocomposite reducing the spacing between the conductive particles.

LM-based antennas present reversible deformability upon mechanical deformations, self-healing capabilities, frequency tuneability *via* stretching and can also act as remote strain sensors.<sup>187,188</sup> LM-based antennas are typically formed by injecting LMs into elastomers, but can also be synthesized from the mechanical merging of LM nanodroplets encased into elastomeric microchannels.<sup>150</sup>

**Gases and vapors sensing.** Semiconducting metal oxides can be used to sense oxidizing and reducing gases *via* chemisorption mechanisms at elevated temperatures.<sup>189</sup> However, at low temperatures these interactions can be associated to physisorption. For example, in presence of oxygen (O<sub>2</sub>) and above 800 °C, the resistivity of Ga<sub>2</sub>O<sub>3</sub> thin films changes as the O<sub>2</sub> concentration increases in the material.<sup>190,191</sup> Galinstan micro and nanodroplets, presenting a native skin of semiconducting amorphous Ga<sub>2</sub>O<sub>3</sub>, allowed for the low temperature sensing of nitrogen dioxide (NO<sub>2</sub>), ammonia (NH<sub>3</sub>) and methane (CH<sub>4</sub>) gases below 150 °C *via* a proposed physisorption mechanism.<sup>192</sup> Doping and mixtures of Ga<sub>2</sub>O<sub>3</sub>-based materials were also shown to enhance and tune the gas sensing

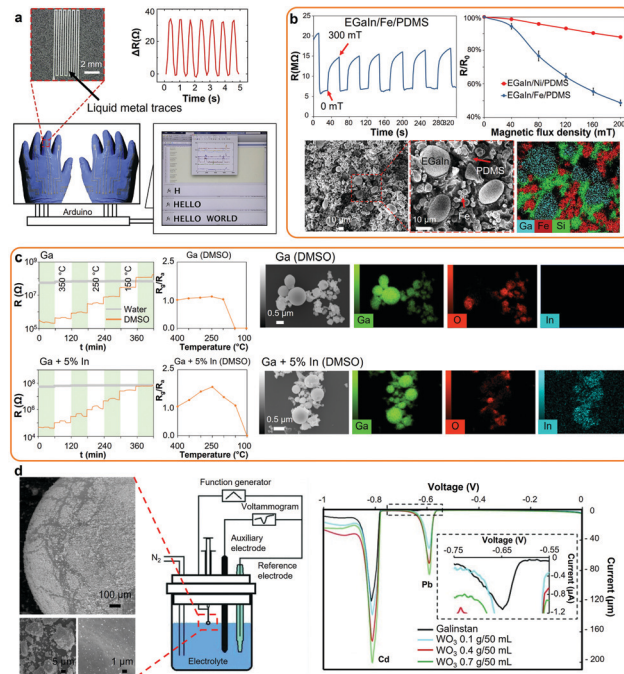


Fig. 6 (a) Photo of a LM-based strain sensor with corresponding electrical signals from finger bending and straightening, and LM integrated sensors in wearable gloves functioning as keyboard. Adapted with permission.<sup>6</sup> Copyright 2018, Elsevier. (b) Response of magnetic LM composites to magnetic field with cyclic resistance changes of the LM/Fe composite, resistance changes of the Fe and Ni LM composites and corresponding SEM and SEM/EDS images of LM/Fe magnetic composites. Adapted with permission.<sup>16</sup> Copyright 2019, Springer Nature. (c) Response and response factors of the Ga and GaIn-based sensors made in DMSO or Milli-Q water post-annealing towards NO<sub>2</sub>, and SEM/EDS elemental mapping of the nanodroplets. Adapted with permission.<sup>22</sup> Copyright 2020, ACS Publications. (d) SEM images of the Galinstan-based heavy metal ion sensor showing the WO<sub>3</sub> surface nanostructures, experimental setup and differential pulse voltammograms of Pb<sup>2+</sup> and Cd<sup>2+</sup> (10 mmol L<sup>-1</sup> each) obtained on the Galinstan(bulk)/WO<sub>3</sub>(nano) electrode as a function of initial WO<sub>3</sub> concentration during LM marble synthesis. Adapted with permission.<sup>26</sup> Copyright 2012, Wiley-VCH.

properties *via* the formation of specific heterostructures at the contact between the Ga<sub>2</sub>O<sub>3</sub> phase and the dopant materials.<sup>189,191,193,194</sup> LM-based processes, such as low temperature alloying and transformation at the nanoscale, can also be used for controlling the doping into metal oxides of post-transition metals that can be used for sensing applications. In one example, the formation of binary GaIn, GaSn and GaZn micro and nanodroplets, and secondary annealing step, was investigated for sensing NO<sub>2</sub> and hydrogen (H<sub>2</sub>).<sup>22</sup> Metal oxides obtained from binary Ga-based nanodroplets were seen to greatly influence the gas sensing properties due to the formation of specific morphologies, particle size, grain and crystal structures. The response and response factors of post-annealed Ga and GaIn-based sensors towards NO<sub>2</sub> and their SEM images and EDS elemental mappings are presented in Fig. 6c. In another example, EGaIn/WO<sub>3</sub> nanocomposites were assembled into gas sensing devices which presented selective chemisorption sensing for H<sub>2</sub> as compared to NO<sub>2</sub> and

hydrogen sulfide ( $\text{H}_2\text{S}$ ).<sup>138</sup> In addition, physisorptive sensors can also be established from composites with post-transition metals. For examples, EGaIn/PANI and EGaIn-based/polydopamine nanocomposites were reported for the sensing of acid vapors and  $\text{NO}_2$  *via* changes in the material conductivities, respectively, at room temperature.<sup>18,100</sup> Gas sensing materials can also be synthesized at the surface of LMs.<sup>56,72</sup> For example,  $\text{Bi}_2\text{O}_3$ -doped SnO nanosheets with controlled  $\text{Bi}_2\text{O}_3$  doping showed selective conductivity responses to  $\text{NO}_2$  and  $\text{H}_2$ .<sup>56</sup>

**Heavy metal ions sensing.** LMs have historically played important roles in the sensing of ions, especially heavy metal ions, in solution, likely due to similarities in the atomic orbitals of post-transition metals and heavy metal ions.<sup>195,196</sup> Such sensors are generally based on stripping voltammetry in which the target ions are preconcentrated into LMs, by applying a negative voltage, and then oxidized when the voltage is reversed and the current is measured. The most common LM used as the electrode for stripping voltammetry is Hg. However due to Hg toxicity, other solid and liquid post-transition metal electrodes are being investigated including Ga, EGaIn and Galinstan.<sup>26,195</sup> Increasing the surface to volume ratio of the electrode can increase the sensitivity for such sensors and various methods have been used for implementing nanostructures within the context of LMs for such applications. As an example, Galinstan(bulk)/ $\text{WO}_3$ (nano) LM marbles were utilized for sensing  $\text{Pb}^{2+}$  and  $\text{Cd}^{2+}$ .<sup>26</sup> The LM marbles presented enhanced sensitivity to  $\text{Pb}^{2+}$  and  $\text{Cd}^{2+}$  as compared to plain unmodified Galinstan due to increased surface area and interfacial amplification of the electrical field that were gained through incorporating  $\text{WO}_3$  nanoparticles onto the surface of the LM. The structure of the LM marble, the experimental setup and differential pulse voltammograms of  $\text{Pb}^{2+}$  and  $\text{Cd}^{2+}$  are shown in Fig. 6d. In another example,  $\text{WO}_3$  nanoparticles were coated on Galinstan nanodroplets for the sensing of  $\text{Pb}^{2+}$ .<sup>197</sup> Here, they both increased the surface to volume ratio and also stabilized the micro and nanodroplets of LMs. Tannic acid-functionalized EGaIn nanodroplets were also demonstrated for the electrochemical sensing of heavy metal ions.<sup>46</sup>

**Plasmonic-based sensing materials.** LMs and LM nanodroplets show promise as plasmonic structures with tunable optical absorption in the UV, visible and near-IR (NIR) ranges.<sup>198–200</sup> Liquid Ga nanodroplets were previously demonstrated as plasmonic materials which exhibit size-dependent resonances spanning from the UV to the NIR.<sup>201,202</sup> In addition, EGaIn nanodroplet suspensions have been shown to demonstrate both strong UV and visible range plasmonic resonance.<sup>200,203</sup> Plasmonic properties of LMs can also be used together with metal oxides. Galinstan/ $\text{Ga}_2\text{O}_3$  LM/metal oxide (LM/MO) micro to nanostructures were also demonstrated to have plasmonic responses that can be tuned depending on the size of the LM droplets.<sup>197</sup> In addition, solidification nanopatterns observed on the surface of dilute BiGa and AgGa LM alloys were demonstrated as plasmonic structures for surface-enhanced Raman spectroscopy.<sup>7</sup>

**Biosensing.** LM nanodroplets present many opportunities for biosensing due to their surface chemistry, plasmonic and electrochemical properties.<sup>203–205</sup> As discussed previously

nanostructured Ga-based materials exhibit tunable resonance energy from the UV to the IR range, as a function of their shapes and sizes.<sup>200,204,205</sup> As biosensing examples, Ga nanodroplets were reported for the sensing of DNA sequences and other molecules.<sup>204,206</sup> In addition, LM nanodroplets can be tracked *in vivo*.<sup>101,107,207–211</sup> Biosensing using fluorescent Ga-based crystallite nanostructures, such as GaN, has also been reported.<sup>91,212,213</sup>

### 4.3 Catalysis

LMs for catalysis present many advantages due to their liquid and dynamic interfaces which are resistant to deactivation (coking) and morphological changes as compared to solid catalysts.<sup>8,49,214</sup> In addition, liquid Ga is an important soft substrate for catalytic transition and other rare and/or expensive elements. The application of bulk post-transition LMs for thermal catalysis and electrocatalysis, such as for gas conversion, will not be reported in this review as they were recently reviewed elsewhere.<sup>49</sup> LMs, either in bulk or nano morphologies, have been used with nano oxide particles as co-contributors for photocatalysis.<sup>197,215</sup> LM micro and nanodroplets were also *in situ* synthesized and demonstrated as sonochemical catalysts for the degradation of organic dyes.<sup>216</sup> LMs can also be used with other metals to enhance catalysis. Liquid Ga and Galinstan with Ce nanoparticles were demonstrated as catalysts resistant to coking for carbon dioxide ( $\text{CO}_2$ ) electro-reduction due to the low van der Waals force at the liquid interface between the LM and the solid carbon products (Fig. 7a).<sup>8</sup> In another example, a mechanically-induced catalytic process using a suspension of Ga nanodroplets and Ag/Ga intermetallic nanorods were utilized for the reduction of  $\text{CO}_2$  into solid carbonaceous products and  $\text{O}_2$  at room temperature.<sup>217</sup> GaPt nanoparticles created by galvanic replacement have also been used for the oxidation of methanol and

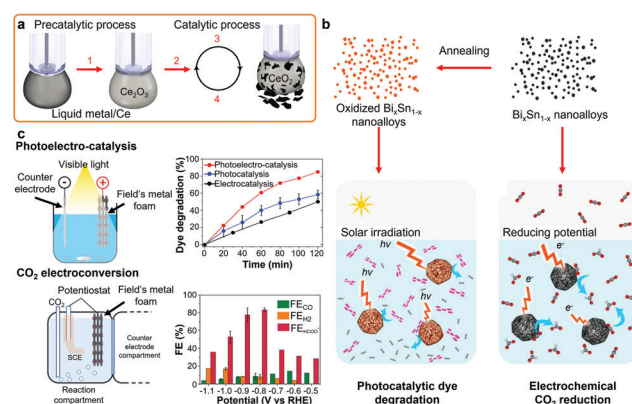


Fig. 7 (a) Room temperature catalytic process of  $\text{CO}_2$  reduction to solid carbon on LM/Ce electrodes. Adapted with permission.<sup>8</sup> Copyright 2019, Springer Nature. (b) Schematics representing the solidified BiSn nanoalloys utilized for photocatalytic dye degradation or  $\text{CO}_2$  electrochemical reduction. Adapted with permission.<sup>19</sup> Copyright 2019, Springer Nature. (c) Photoelectrocatalysis and  $\text{CO}_2$  electrochemical conversion using a metallic foam formed from the assembly of Field's metal nanodroplets and corresponding dye degradation and  $\text{CO}_2$  conversion rates, respectively. Adapted with permission.<sup>23</sup> Copyright 2019, Wiley-VCH.

ethanol.<sup>218</sup> In another report, a GaPt catalytic system was prepared by galvanic replacement of Pt salts on Ga on an alumina matrix for propane dehydrogenation at 350 to 450 °C.<sup>219</sup> Pd has also been used with a Ga support for dehydrogenation of organic compounds at elevated temperatures.<sup>214</sup>

Nanoparticles obtained using various LM solidification processes also present attractive catalytic properties due to the controllable polycrystallinity, grain sizes, nanodomains and surface oxide decoration.<sup>19,23,28,115</sup> For example, eutectic BiSn nanoalloys showed higher photocatalytic and electrocatalytic performance as compared to non-eutectic BiSn nanoalloys, for the degradation of organic dyes and CO<sub>2</sub> reduction reaction, respectively.<sup>23</sup> The schematic representation of the solidified BiSn nanoalloys and their catalytic applications are presented in Fig. 7b. The specific formation of catalytic surface oxides, such as mixed In<sub>2</sub>O<sub>3</sub>, SnO and SnO<sub>2</sub> nanocrystals, was also demonstrated during the foaming and solidification of Field's metal nanodroplets for the photoelectrocatalysis of organic dyes and CO<sub>2</sub> electrochemical reduction as presented in Fig. 7c.<sup>19</sup>

Oxidation of LM micro and nanodroplets can also lead to the formation of catalytically active nanomaterials.<sup>90,197</sup> As an example, hexagonal  $\alpha$ -Ga<sub>2</sub>O<sub>3</sub> nanoflakes with photocatalytic activity have been prepared by the sonication of liquid Ga for up to 60 minutes in DI water followed by annealing.<sup>90</sup> In addition, LM nanocomposites were shown to present high photocatalytic activity.<sup>70,136,137,215</sup> For example, EGaIn/MnO<sub>2</sub> nanocomposites presented high photocatalytic activity for the degradation of organic dyes.<sup>70</sup>

#### 4.4 Energy applications

**Energy storage devices.** Post-transition metals and alloys are increasingly considered as electrode materials in LM batteries, electrode nanocomposites in lithium-ion and sodium-ion batteries and as conductive media. Sn and Ga present high theoretical specific capacity of 990 mA h g<sup>-1</sup> and 769 mA h g<sup>-1</sup>, for the discharge products of Li<sub>2</sub>Ga and Li<sub>x</sub>Sn (0 ≤ x ≤ 4.4), respectively.<sup>220,221</sup> In particular, Ga shows exceptional lithiation properties as one Ga atom can host two lithium atoms, and potentially presents self-healing properties during lithiation/delithiation cycles.<sup>4,220,222</sup> During lithiation, liquid to solid phase transition occurs with the formation of LiGa alloys and particularly of Li<sub>2</sub>Ga, which is a solid product with a melting point of ~288 °C. The lithiation process of a Ga nanodroplet (~300 nm) is shown in Fig. 8a.<sup>4</sup> Similarly, Ga can form NaGa alloys during sodiation cycles. Ga shows a theoretical capacity of 217 mA h g<sup>-1</sup> with the formation of Na<sub>22</sub>Ga<sub>39</sub>, while it should be considered that GaNa phases require very high temperature for melting.<sup>223</sup> Altogether, lithiation and sodiation are associated with the loss of the liquid/liquid interface and important volume expansion, of up to ~160% and ~260% respectively, which remains problematic for the mechanical stability of the electrode material.<sup>4,224</sup>

LM batteries typically refer to batteries operating at high (above 400 °C) or intermediate (240 °C) temperatures which consist of two high melting point LM electrodes separated by a molten salt electrolyte.<sup>223,225</sup> LM batteries show superior electrode charge-transfer kinetics due to their liquid/liquid

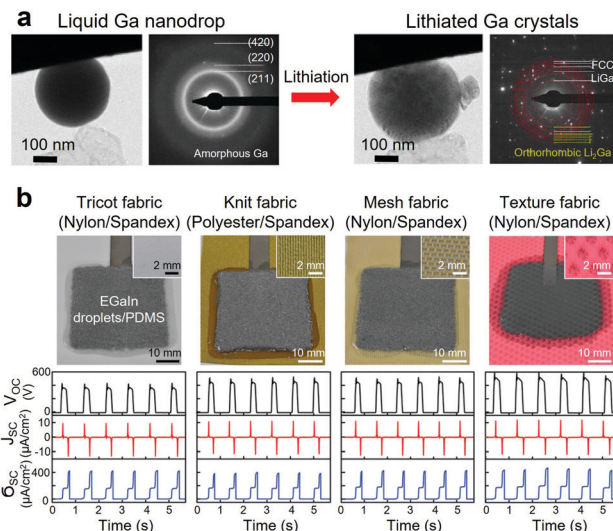


Fig. 8 (a) Phase transformation of an amorphous liquid Ga nanodrop before and after lithiation (TEM images). Adapted with permission.<sup>4</sup> Copyright 2013, ACS Publications. (b) Wearable triboelectric nanogenerator based on EGaIn/PDMS elastomer composite integrated with stretchable fabrics and corresponding electrical outputs. Adapted with permission.<sup>13</sup> Copyright 2020, Wiley-VCH.

interfaces, are immune to dendrite formation due to the solubility of the deposited species, possess long lifetimes and low cost depending on the metals and alloys chosen, but require high temperature operation and can only be used for static storage in large scale applications.<sup>225–227</sup> The advances and current understanding of LM batteries were recently reviewed elsewhere.<sup>223</sup> Ga-Based room temperature LM batteries were also reported, which present many advantages in terms of thermal management and reduction of parasitic reactions that occur at high temperatures.<sup>223</sup> Room temperature LM batteries can also be applied to portable and soft electronics due to the stretchability of the LMs. Nanostructures in the LM type electrolytes can potentially play an important role for enhancing their properties, a topic that can be widely explored in the future.

Ga-Based liquid alloys have also been used as electrode materials for the development of soft batteries which allowed for some degree of flexibility and stretchability.<sup>228–230</sup> Soft and deformable LM-based supercapacitors were synthesized based on EGaIn or Galinstan films.<sup>231,232</sup> In one example, CNTs were coated on the surface of microtextured EGaIn films on a PDMS substrate to achieve a soft and stretchable supercapacitor which was able to retain its capacitance under 30% strain.<sup>232</sup>

Nanosized Ga-based LM fillers were also investigated for lithium-ion and sodium-ion batteries.<sup>220,233–238</sup> As an example, GaSn nanodroplets stabilized with rGO and CNTs were synthesized as a nanocomposite slurry and coated on Cu foils to form anode materials, which demonstrated self-healing capability and retained capacity after 4000 cycles with a capacity of ~400 mA h g<sup>-1</sup> at 4000 mA g<sup>-1</sup>.<sup>220</sup> In another example, core/shell nanocomposite of LM nanodroplets contained in hollow carbon fibers was investigated to alleviate the volume expansion during lithiation and delithiation cycles.<sup>239</sup>

**Energy harvesting.** Soft LM polymer micro and nanocomposites were investigated as stretchable thermoelectric generators and triboelectric nanogenerators energy harvesting devices.<sup>13,154,240–242</sup> EGaIn-Based elastomers with integrated thermoelectric elements were demonstrated as a stretchable and flexible thermoelectric devices.<sup>240,242</sup> LM/PDMS triboelectric nanogenerator composites (Fig. 8b) were also proposed for harvesting energy from body motions presenting high stretchability (strain limit above 500%).<sup>13</sup> In addition, the ability to mechanically change the surface area of LMs in electrolytes (e.g. hydrogels) was demonstrated and which resulted in variable area capacitors for mechanical-to-electrical energy harvesting.<sup>243</sup> This concept could be further extended to nano-scale LM components.

**Thermal management.** Bulk LMs are excellent thermal management materials due to their high thermal conductivity and liquid interface providing an intimate contact between substrates.<sup>244</sup> LM nanocomposites and nanodroplets were also investigated as thermal pathways for heat dissipation.<sup>2,29,108,110,245,246</sup> For example, a EGaIn LM soft micro/nanocomposite with high maximum strain ( $\sim 600\%$ ) exhibited exceptional thermal conductivity.<sup>2</sup> The thermal conductivity was shown to increase to a metal-like conductivity under strain due to the deformation of the LM droplets forming thermally conductive pathways in the stretching direction.

#### 4.5 Nanomedicine and biomedical applications

Selected post-transition metals and alloys, all based on Ga-based alloys, are liquid within the range of human body temperature, which present an unprecedented opportunity of using metallic fluids for biomedical applications and nanomedicine. Unlike Hg, Ga-based alloys are considered to have a low level of toxicity. As an example of biocompatibility, both Ga and EGaIn were investigated as microelectrodes for neural tissue stimulation.<sup>247</sup> Subsequently, the biocompatibility of the LM microelectrodes was demonstrated on long-term hippocampal neurons cultures.

Ga-Based nanodroplets are increasingly considered as functional biomaterials. The interest in developing functionalized Ga-based nanodroplets lies in the synergies between their LM cores, fluidity and ease of functionalization and synthesis at the nanoscale.<sup>3,208,209,211</sup> Functionalized EGaIn nanodroplets also presented good biodegradability and low toxicity in mice.<sup>3</sup> Functionalized LM nanodroplets can respond to a wide range of physical stimuli including acoustic and electromagnetic waves, light and thermal stimulations and also chemical stimuli for drug delivery, tumor cell treatment, biosensing and bio-imaging as summarized in Fig. 9a.<sup>3,101,181,203,204,207–211,248–250</sup>

It should be considered that during the synthesis of Ga-based nanodroplets *via* mechanical agitation, such as EGaIn, the release of Ga and In ions was reported, which presented significant toxicity to a series of human cell cultures.<sup>251</sup> Washing or functionalization steps post synthesis can alleviate this effect. Compared to Hg or Cd ions, Ga and In ions show much lower toxicity.<sup>251,252</sup> In addition, some Ga salts, such as gallium nitrate ( $\text{Ga}(\text{NO}_3)_3$ ), are authorized drugs and used as an iron(III)

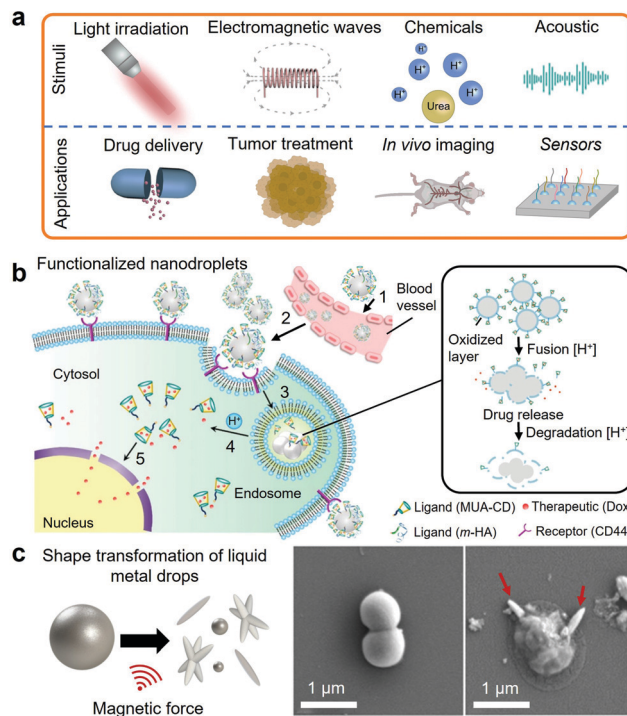


**Fig. 9** (a) Illustration of the reported stimuli and applications of LM nanodroplets in nanomedicine. (b) Illustration of the acid-triggered drug delivery mechanism using functionalized EGaIn nanodroplets. Adapted with permission.<sup>3</sup> Copyright 2015, Springer Nature. (c) Representation of the magnetically induced shape transformation of magnetic LM nanoparticles and SEM images of the bacteria before and after magnetic activation. Adapted with permission.<sup>17</sup> Copyright 2020, ACS Publications.

analogue in cancer therapy and also proposed as therapeutics for the treatment of antibiotic-resistant bacteria, as Ga(III) ions were shown to disrupt the iron-dependent metabolic pathways of bacteria.<sup>253–257</sup> Ga compounds are also routinely used as contrast agents in nuclear medicine and oncology.<sup>248,258</sup> However, we note reports of toxic exposure to Ga complexes, such as halide complexes, and airborne In compounds, related to electronic component manufacturing, that can induce significant toxicity concerns and threat to human health.<sup>259,260</sup>

**Drug delivery and tumor therapy.** The therapeutics application of Ga-based nanodroplets were recently reviewed.<sup>248</sup> The more recent developments of functional nanodroplets for biomedical applications are focused on multi-synergic processes, that take advantage of multifunctional coatings and the metallic properties of the nanodroplets.<sup>107,211</sup> LM nanodroplets have been demonstrated as drug carriers that allow the release of therapeutic agents *via* chemical stimuli, such as in intracellular acidic environments, or *via* physical stimuli, including thermal deformation under NIR irradiation, acoustic or electromagnetic stimulation, or using a combination of chemical and physical stimuli.<sup>3,107,261</sup> As one of the pioneering examples, functionalized EGaIn nanodroplets, with thiolated polymeric shells, were utilized as drug delivery systems, which released the therapeutic molecules after cellular internalization and fusion in the mild acidic conditions (Fig. 9b).<sup>3</sup> Advantageously, the EGaIn



materials also presented enhanced contrast capability for X-ray imaging at the same time. There are many examples of LM nanodroplets functionalized with enzyme, proteins, nanoparticles and polymer coatings that were investigated for tumor therapy.<sup>107,207–209,211,262–265</sup> In many of these examples, the local temperature in the vicinity of the functionalized EGaIn nanodroplets could be remotely increased *via* NIR irradiation providing photothermal therapy both in laboratory and animal models.

**Antimicrobial agent.** Ga-Based nanodroplets were shown to release Ga<sup>3+</sup> ions upon oxidation in acidic and basic environments, which can provide antibacterial properties in biological systems.<sup>251,256</sup> The use of micro and nanodroplets can enhance the diffusion mixing rate of Ga<sup>3+</sup> released from Ga-based materials. To date, LM nanoalloys and stimuli-responsive nanocomposites have been investigated as antimicrobial and biofilms remediation materials.<sup>17,266</sup> Ga nanodroplets (~300 nm) were utilized as adhesive nucleation sites on fabric materials for the formation of GaCu nanoalloys *via* galvanic replacement which presented antibacterial, antifungal and antiviral properties.<sup>266</sup> In another example, the shape transformation of magnetic Galinstan micro and nanodroplets were induced *via* magnetic activation and presented nanosharp edges that physically ruptured bacteria cells and the biofilm matrix (Fig. 9c).<sup>17</sup>

#### 4.6 Other applications

The other applications that utilize the surface tension, solvation, electrical and thermal conductivities, surface functionalization, reflectivity, fluidity, or reactivity of LMs are presented in this section and summarized in Table 4.

**LM-based actuators.** The interfacial tension of LMs can be chemically and electrochemically manipulated for actuation in electrolyte solutions at low voltages, as shown in examples with mm- and sub-mm sized LM drops.<sup>267–273</sup> At the nanoscale,

nanocoating of mm-sized LM drops was shown to drastically affect the surface tension induced forces. As examples, actuation of nanocoated LM marbles was reported *via* electro- and photochemical methods, where the nanocoating altered the surface tension and capacitance of the LM marbles or acted as a photocatalyst triggering a chemical reaction, respectively.<sup>69,143</sup> Soft actuators based on thermally and electrically conductive LM nanocomposites were also developed for soft robotics taking advantage of the deformable and soft nature of the LM nanodroplets, or extrusion ability, incorporated into responsive elastomers.<sup>2,274–277</sup> Particularly, a nanocomposite based on EGaIn nanodroplets and a liquid crystal polymer was demonstrated to provide shape-morphing capabilities *via* electro- or photo-thermal actuation.<sup>278</sup> Adaptive materials, such as liquid crystalline systems, present great opportunities for the development of soft actuators and other functional LM-based nanocomposites.<sup>279–281</sup>

**Magnetic LM fluids.** Magnetic micro and nanoparticles, such as gadolinium (Gd), Ni, Fe, Fe<sub>2</sub>O<sub>3</sub> and neodymium–iron–boron (NdFeB), were incorporated into LMs which provided magnetic properties to the LM phase.<sup>108,124,183,184</sup> In one example, a Gd supersaturated Ga-based LM presented nanoprecipitates of Gd, which enabled the magnetic properties for the base LM alloy and also presented high magnetocaloric effect at room temperature.

**Magnetic LM-based actuators.** Magnetic LM fluids, polymeric, micro and nanocomposites can be magnetically actuated.<sup>142,182–185,282,283</sup> Magnetization and demagnetization cycles were shown to align the dispersed magnetic particles and enable actuation of the nanocomposites with potential applications as magnetic switches and for soft robotic actuation.<sup>47,185</sup> For example, LM soft nanocomposites based on mixed nanosized EGaIn/Fe<sub>3</sub>O<sub>4</sub> nanoparticles showed combined remote magnetic actuation capabilities and high electrical conductivity.<sup>47</sup>

Table 4 Other applications of nanostructured LMs

Application	LM	Media	Ref.
LM-based actuators	EGaIn and Galinstan droplet LM marbles LM composites	Electrolyte, H <sub>2</sub> O <sub>2</sub> solution, polymer matrix	2, 69, 143, 268, 270, 271 and 274
Magnetic fluids and LM-based actuators	EGaIn/Ni EGaIn/NdFeB Ga/Ni Galinstan/Fe Galinstan/Gd LM marble	Air, polymer matrix	47, 108, 182–186 and 283
EMI shielding	EGaIn EGaIn/Ni Ga/rGO	Polymer matrix LM composite	29 and 284–287
Micromirrors	Galinstan EGaIn	Electrolyte	288 and 289
Separation	Field's metal In and Ga oxides EGaIn/PANI	Electrolyte, polymer matrix	18, 19 and 290
Thermal management	Functionalized Ga EGaIn Ga/Cu composite Ga/diamond composite Galinstan/Gd	Silicone oil, air, polymer matrix	2, 29, 108, 110 and 244–246
Nanothermometers	Ga/CNTs	Vacuum	291 and 292
Nanomaterial synthesis using LMs	Ga alloys	Electrolytes	22 and 293–296

**EMI shielding.** LM composites and nanocomposites were investigated as stretchable electromagnetic interference (EMI) shielding materials which could provide both high electrical and thermal conductivities.<sup>284–287</sup> The LM phase can act as a continuous conductive phase absorbing and efficiently dissipating the incoming electromagnetic waves, as the mixed matrix surface enhanced the electromagnetic waves reflection. As an example, a LM-based EGaIn/Ni micro/nanocomposite was coated on various stretchable substrates for added EMI shielding properties.<sup>287</sup> In another example, a EGaIn elastomer composite was synthesized by mechanically mixing bulk EGaIn into a PDMS base to provide EMI shielding at low temperatures.<sup>284</sup>

**Micromirrors.** Reflective LM surfaces present useful properties for optical applications, particularly with the dynamic control of their surfaces that allow switching between concave and convex shapes at the milli- and micrometer scales.<sup>289</sup> Micromirrors and micromirrors array with tunable reflectivity were demonstrated with a dimension of 100  $\mu\text{m}$ .<sup>288</sup> The formation of nanomirrors from LM traces and nanodroplets remains to be demonstrated.

**Separation.** LMs and post-transition metals can be used for the synthesis of size exclusion or ionic separation materials thanks to their ease of synthesis into porous and mixed polymeric structures, and to their interactions with alkali and heavy metal ions. As an example of a size separation material, solidified Field's metal nanodroplets were sintered by a mild exothermic chemical reaction into microporous foam structures.<sup>19</sup> In another example, lithium ion selective nanocomposites were also formed *via* the *in situ* dealloying of EGaIn

nanodroplets in a polymeric matrix.<sup>290</sup> The dealloying products, Ga oxides and In metal nanoparticles, provided selective binding sites for  $\text{Li}^+$  and mechanical cohesion to the polymer nanocomposites, respectively.

**Nanothermometers.** Ga can be confined at the nanoscale within carbon nanotubes (diameter between 40 to 200 nm), which were utilized as nanothermometers operating between  $-80\text{ }^\circ\text{C}$  and  $500\text{ }^\circ\text{C}$ .<sup>291,292</sup> Such concepts can be extended for the formation of many other thermally sensitive functional nanodevices.

**Nanomaterials synthesis using LMs.** Collection of the oxide layer of LMs was shown to yield a range of functional low-dimensional materials as previously presented in Section 2.2. LM-based synthesis of inorganic nanomaterials can also be achieved *via* the controlled thermal, electrochemical or acoustic expulsion of alloyed and dissolved elements in LMs.<sup>22,293,294,296,297</sup> For example, fast electrochemical perturbations in the surface tension of Ga-based LM alloys can trigger the expulsion of alloyed elements, such as Sn, In, Bi and Zn from the LM base into nanostructured metallic or metal oxide materials.<sup>293,295</sup> A few major examples regarding different methods for preparing nanomaterials from LM alloys are presented in Table 5.

## 5. Conclusion and future perspectives

In this review, we reported the advances of room temperature and low melting point LMs and alloys in nanotechnology. We showed that the core and surface of LMs can be engineered

Table 5 Nanomaterials synthesis using LMs

Method	LM	Advantages and disadvantages	Collected materials and references
Touch-print	Ga-Based and molten post-transition metals and alloys	Limited to favorably formed oxides, heterostructure formation, thermal post-treatment transformation, substrate-dependent, possible LM residues	$\text{Ga}_2\text{O}_3$ <sup>50,68</sup> $\text{HfO}_2$ , $\text{Al}_2\text{O}_3$ , $\text{Gd}_2\text{O}_3$ <sup>50</sup> $\text{SnO}$ <sup>43</sup> $\text{Bi}_2\text{O}_3$ <sup>44</sup> $\text{SnO}/\text{In}_2\text{O}_3$ heterostructures <sup>298</sup> $\text{Bi}_2\text{O}_3$ doped $\text{SnO}$ <sup>56</sup> $\text{Sb}_2\text{O}_3$ <sup>57</sup> $\text{ZnO}$ <sup>299,300</sup> $\text{Ga}_2\text{O}_3$ <sup>62,63,65–67,301,302</sup> $\text{In}_2\text{O}_3$ <sup>65</sup> $\text{PbO}$ <sup>303</sup> $\text{ITO}$ <sup>55</sup> $\text{SnO}$ <sup>65</sup> $\text{Ga}_2\text{O}_3$ <sup>64</sup> $\text{HfO}_2$ , $\text{Ga}_2\text{O}_3$ <sup>50</sup> $\text{TiO}_2$ <sup>61</sup> $\text{CoO}_x$ <sup>60</sup> $\text{SnO}$ and $\text{SnO}_x$ <sup>58,59</sup> $\text{MnO}_2$ <sup>70</sup> $\text{Mn}_3\text{O}_4$ <sup>297</sup> $\text{MoS}_2$ <sup>71,297</sup> $\text{Bi}_2\text{Te}_3$ <sup>72</sup> $\text{CuO}$ , $\text{Cu}_2\text{O}$ and $\text{Cu}$ <sup>137</sup> Carbon materials <sup>296,297</sup> Layered double oxides <sup>73</sup> $\text{Sn}$ , $\text{ZnO}$ , $\text{In}/\text{In}_2\text{O}_3$ , $\text{Bi}/\text{Bi}_2\text{O}_3$ nanostructures <sup>293,295</sup>
Stamping, squeezing, patterning and spreading	Ga-Based and molten post-transition metals and alloys		
Agitation	Ga-Based alloys	High yield	
Gas injection	Ga-Based and molten post-transition metals and alloys	Access to favorably and non-favorably formed oxides	
Surface templating and reactive methods	Ga-Based alloys	Near room temperature reactive process, formation of monolayers and crystals, limited to specific ionic precursors and solvent environments, thermal post-treatment transformation	

at the nanoscale to offer fascinating solid/liquid core/shell structures, nanoparticle inclusions, surface decorations and nanopatterns, and deviate from the formation of thermodynamically favored metal oxides during mechanical agitation.

The synthesis of LM nanodroplets is of particular interest due to the low melting points of the post-transition metals and alloys that allow processing under mild mechanical conditions. However, the realization of nanodroplets with a narrow size distribution and which are liquid at the sub-10 nm scales still represents a significant challenge. To date still relatively few binary and ternary LM systems have been investigated at the nanoscale. Many possibilities of multi-elemental LM nanoalloys and high entropy liquid alloys are yet to be investigated with the potential for machine learning approaches leading to materials with exciting new properties.

LM based nanocomposites can be designed to present enhanced mechanical properties, electrical and thermal conductivities, as well as hybrid capabilities. The LMs can act as reactive phases to solvate nanoadditives and participate in their chemical reactions. Such capabilities also highlight the widely expanded usages of LMs as liquid media for physicochemical transformations of solutes at the nanoscale.

LMs are used in soft electronic components due to their intrinsic stretchability characteristics. Nanoscale patterning of LM traces and wires are currently limited to advanced lithography techniques with the best reported resolution of ~180 nm. However, LM nanodroplets in composites can potentially offer better resolution traces. Advantageously, LM nanodroplets can be particularly well integrated with elastomers for soft electronic applications. Nevertheless, for the development of such advanced soft electronics, the controlled dispersion and specific interfacial compatibility of LM nanodroplets within polymers remain to be fully investigated.

LMs and solidified LMs present many opportunities for catalytic applications at the nanoscale. Nano-dimensional LMs have been shown to exhibit a good degree of catalytic activity and can be used as soft supports to other catalytic and reactive elements, while presenting nonpolar liquid interfaces resistant to deactivation and coking. However, understanding the surface elemental distribution still needs to be addressed for the synthesis of catalytic LM alloys. Solidified nano-dimensional LMs, made from LM synthesis processes, also present many advantages for creating highly catalytically active nanostructures with engineered oxide representation. However, solidification mechanisms leading to catalytically favorable morphologies and crystal phases remain to be uncovered.

Nanostructured LMs also show potential for the development of the next generation of flexible energy storage devices both as components of electrodes and electrolytes. Some challenges remain, such as control of the volume expansion during charge/discharge cycles, increasing the charge capacity of the systems and understanding the interfacial electrochemical reactions. LM nanodroplets also enable wearable energy harvesting devices, such as using triboelectric nanogenerators, that are based on the fluidity and softness of the LMs. The next generation of LM nanocomposites will witness their integration into more

multifunctional devices integrating energy generation, electronic, sensing and actuation capabilities.

Finally, selected Ga-based LM nanodroplets present great opportunities in biotechnology and nanomedicine due to their low toxicity and liquid states below or at the temperature of the human body. Such Ga based LM nano entities offer the opportunities of becoming platforms for the design of multifunctional nanodevices with synergetic functionalities for drug delivery, cancer therapy and imaging. To date, the inclusion of many other inorganic and metallic elements in the Ga-based LM based bio-systems has not been investigated, which would offer new synergetic effects for enhanced imaging, sensing and therapeutic capabilities.

## Author contributions

Francois-Marie Allieux: writing – original draft, and review and editing. Mohammad B. Ghasemian: writing – original draft. Wanjie Xie: writing – original draft. Anthony P. O'Mullane: review and editing. Torben Daeneke: review and editing. Michael D. Dickey: review and editing. Kouros Kalantar-Zadeh: supervision, writing – original draft, and review & editing.

## Conflicts of interest

There are no conflicts to declare.

## Acknowledgements

The authors would like to acknowledge the Australian Research Council (ARC) Laureate Fellowship grant (FL180100053) for financial support for this work.

## References

- 1 M. Losurdo, A. Suvorova, S. Rubanov, K. Hingerl and A. S. Brown, *Nat. Mater.*, 2016, **15**, 995–1002.
- 2 M. D. Bartlett, N. Kazem, M. J. Powell-Palm, X. Huang, W. Sun, J. A. Malen and C. Majidi, *Proc. Natl. Acad. Sci. U. S. A.*, 2017, **114**, 2143–2148.
- 3 Y. Lu, Q. Hu, Y. Lin, D. B. Pacardo, C. Wang, W. Sun, F. S. Ligler, M. D. Dickey and Z. Gu, *Nat. Commun.*, 2015, **6**, 10066.
- 4 W. Liang, L. Hong, H. Yang, F. Fan, Y. Liu, H. Li, J. Li, J. Y. Huang, L.-Q. Chen, T. Zhu and S. Zhang, *Nano Lett.*, 2013, **13**, 5212–5217.
- 5 J. Ma, Y. Lin, Y.-W. Kim, Y. Ko, J. Kim, K. H. Oh, J.-Y. Sun, C. B. Gorman, M. A. Voinov, A. I. Smirnov, J. Genzer and M. D. Dickey, *ACS Macro Lett.*, 2019, **8**, 1522–1527.
- 6 L. Tang, S. Cheng, L. Zhang, H. Mi, L. Mou, S. Yang, Z. Huang, X. Shi and X. Jiang, *iScience*, 2018, **4**, 302–311.
- 7 J. Tang, S. Lambie, N. Meftahi, A. J. Christofferson, J. Yang, M. B. Ghasemian, J. Han, F.-M. Allieux, M. A. Rahim, M. Mayyas, T. Daeneke, C. F. McConville, K. G. Steenbergen, R. B. Kaner, S. P. Russo, N. Gaston and K. Kalantar-Zadeh, *Nat. Nanotechnol.*, 2021, **16**, 431–439.

- 8 D. Esrafilzadeh, A. Zavabeti, R. Jalili, P. Atkin, J. Choi, B. J. Carey, R. Brkljača, A. P. O'Mullane, M. D. Dickey, D. L. Officer, D. R. MacFarlane, T. Daeneke and K. Kalantar-Zadeh, *Nat. Commun.*, 2019, **10**, 865.
- 9 E. J. Markvicka, R. Tutika, M. D. Bartlett and C. Majidi, *Adv. Funct. Mater.*, 2019, **29**, 1900160.
- 10 M. J. Regan, E. H. Kawamoto, S. Lee, P. S. Pershan, N. Maskil, M. Deutsch, O. M. Magnussen, B. M. Ocko and L. E. Berman, *Phys. Rev. Lett.*, 1995, **75**, 2498–2501.
- 11 P. S. Pershan, *J. Appl. Phys.*, 2014, **116**, 222201.
- 12 S.-F. Tsay and S. Wang, *Phys. Rev. B: Condens. Matter Mater. Phys.*, 1994, **50**, 108–112.
- 13 C. Pan, D. Liu, M. J. Ford and C. Majidi, *Adv. Mater. Technol.*, 2020, **5**, 2000754.
- 14 S.-Y. Tang, D. R. G. Mitchell, Q. Zhao, D. Yuan, G. Yun, Y. Zhang, R. Qiao, Y. Lin, M. D. Dickey and W. Li, *Matter*, 2019, **1**, 192–204.
- 15 A. Fang, C. Adamo, S. Jia, R. J. Cava, S.-C. Wu, C. Felser and A. Kapitulnik, *Sci. Adv.*, 2018, **4**, eaaq0330.
- 16 G. Yun, S.-Y. Tang, S. Sun, D. Yuan, Q. Zhao, L. Deng, S. Yan, H. Du, M. D. Dickey and W. Li, *Nat. Commun.*, 2019, **10**, 1300.
- 17 A. Elbourne, S. Cheeseman, P. Atkin, N. P. Truong, N. Syed, A. Zavabeti, M. Mohiuddin, D. Esrafilzadeh, D. Cozzolino, C. F. McConville, M. D. Dickey, R. J. Crawford, K. Kalantar-Zadeh, J. Chapman, T. Daeneke and V. K. Truong, *ACS Nano*, 2020, **14**, 802–817.
- 18 C. Zhang, F.-M. Allieux, M. A. Rahim, J. Han, J. Tang, M. B. Ghasemian, S.-Y. Tang, M. Mayyas, T. Daeneke, P. Le-Clech, R. B. Kaner, D. Esrafilzadeh and K. Kalantar-Zadeh, *Chem. Mater.*, 2020, **32**, 4808–4819.
- 19 F.-M. Allieux, S. Merhebi, J. Tang, S. A. Idrus-Saidi, R. Abbasi, M. G. Saborio, M. B. Ghasemian, J. Han, R. Namivandi-Zangeneh, A. P. O'Mullane, P. Koshy, R. Daiyan, R. Amal, C. Boyer and K. Kalantar-Zadeh, *Adv. Funct. Mater.*, 2020, **30**, 1907879.
- 20 E. J. Markvicka, M. D. Bartlett, X. Huang and C. Majidi, *Nat. Mater.*, 2018, **17**, 618–624.
- 21 K. Kalantar-Zadeh, J. Tang, T. Daeneke, A. P. O'Mullane, L. A. Stewart, J. Liu, C. Majidi, R. S. Ruoff, P. S. Weiss and M. D. Dickey, *ACS Nano*, 2019, **13**, 7388–7395.
- 22 S. A. Idrus-Saidi, J. Tang, J. Yang, J. Han, T. Daeneke, A. P. O'Mullane and K. Kalantar-Zadeh, *ACS Sens.*, 2020, **5**, 1177–1189.
- 23 J. Tang, R. Daiyan, M. B. Ghasemian, S. A. Idrus-Saidi, A. Zavabeti, T. Daeneke, J. Yang, P. Koshy, S. Cheong, R. D. Tilley, R. B. Kaner, R. Amal and K. Kalantar-Zadeh, *Nat. Commun.*, 2019, **10**, 4645.
- 24 J. Yan, M. H. Malakooti, Z. Lu, Z. Wang, N. Kazem, C. Pan, M. R. Bockstaller, C. Majidi and K. Matyjaszewski, *Nat. Nanotechnol.*, 2019, **14**, 684–690.
- 25 S. Liu, M. C. Yuen, E. L. White, J. W. Boley, B. Deng, G. J. Cheng and R. Kramer-Bottiglio, *ACS Appl. Mater. Interfaces*, 2018, **10**, 28232–28241.
- 26 V. Sivan, S.-Y. Tang, A. P. O'Mullane, P. Petersen, N. Eshtiaghi, K. Kalantar-zadeh and A. Mitchell, *Adv. Funct. Mater.*, 2013, **23**, 144–152.
- 27 C. J. Thrasher, Z. J. Farrell, N. J. Morris, C. L. Willey and C. E. Tabor, *Adv. Mater.*, 2019, **31**, 1903864.
- 28 F.-M. Allieux, S. Merhebi, M. B. Ghasemian, J. Tang, A. Merenda, R. Abbasi, M. Mayyas, T. Daeneke, A. P. O'Mullane, R. Daiyan, R. Amal and K. Kalantar-Zadeh, *Nano Lett.*, 2020, **20**, 4403–4409.
- 29 C. Wang, Y. Gong, B. V. Cuning, S. Lee, Q. Le, S. R. Joshi, O. Buyukcakir, H. Zhang, W. K. Seong, M. Huang, M. Wang, J. Lee, G.-H. Kim and R. S. Ruoff, *Sci. Adv.*, 2021, **7**, eabe3767.
- 30 R. Tutika, A. B. M. T. Haque and M. D. Bartlett, *Commun. Mater.*, 2021, **2**, 64.
- 31 V. Kamysbayev, N. M. James, A. S. Filatov, V. Srivastava, B. Anasori, H. M. Jaeger, Y. Gogotsi and D. V. Talapin, *ACS Nano*, 2019, **13**, 12415–12424.
- 32 T. Daeneke, K. Khoshmanesh, N. Mahmood, I. A. de Castro, D. Esrafilzadeh, S. J. Barrow, M. D. Dickey and K. Kalantar-Zadeh, *Chem. Soc. Rev.*, 2018, **47**, 4073–4111.
- 33 F. Krisnadi, L. L. Nguyen, Ankit, J. Ma, M. R. Kulkarni, N. Mathews and M. D. Dickey, *Adv. Mater.*, 2020, **32**, 2001642.
- 34 T. R. Lear, S.-H. Hyun, J. W. Boley, E. L. White, D. H. Thompson and R. K. Kramer, *Extreme Mech. Lett.*, 2017, **13**, 126–134.
- 35 M. J. Regan, P. S. Pershan, O. M. Magnussen, B. M. Ocko, M. Deutsch and L. E. Berman, *Phys. Rev. B: Condens. Matter Mater. Phys.*, 1996, **54**, 9730–9733.
- 36 K. S. Vahvaselkä, *Phys. Scr.*, 1980, **22**, 647–652.
- 37 C. J. Powell, *Adv. Phys.*, 1967, **16**, 203–213.
- 38 O. G. Shpyrko, A. Y. Grigoriev, C. Steimer, P. S. Pershan, B. Lin, M. Meron, T. Graber, J. Gerbhardt, B. Ocko and M. Deutsch, *Phys. Rev. B: Condens. Matter Mater. Phys.*, 2004, **70**, 224206.
- 39 M. J. Regan, H. Tostmann, P. S. Pershan, O. M. Magnussen, E. DiMasi, B. M. Ocko and M. Deutsch, *Phys. Rev. B: Condens. Matter Mater. Phys.*, 1997, **55**, 10786–10790.
- 40 M. D. Dickey, *ACS Appl. Mater. Interfaces*, 2014, **6**, 18369–18379.
- 41 J. F. García Martín, S. Sánchez and R. Metz, *Oxid. Met.*, 2012, **77**, 1–7.
- 42 E. Ricci, T. Lanata, D. Giuranno and E. Arato, *J. Mater. Sci.*, 2008, **43**, 2971–2977.
- 43 T. Daeneke, P. Atkin, R. Orrell-Trigg, A. Zavabeti, T. Ahmed, S. Walia, M. Liu, Y. Tachibana, M. Javaid, A. D. Greentree, S. P. Russo, R. B. Kaner and K. Kalantar-Zadeh, *ACS Nano*, 2017, **11**, 10974–10983.
- 44 K. A. Messalea, B. J. Carey, A. Jannat, N. Syed, M. Mohiuddin, B. Y. Zhang, A. Zavabeti, T. Ahmed, N. Mahmood, E. Della Gaspera, K. Khoshmanesh, K. Kalantar-Zadeh and T. Daeneke, *Nanoscale*, 2018, **10**, 15615–15623.
- 45 K. Tiwari, M. Manolata Devi, K. Biswas and K. Chattopadhyay, *Prog. Mater. Sci.*, 2021, **121**, 100794.
- 46 M. A. Rahim, F. Centurion, J. Han, R. Abbasi, M. Mayyas, J. Sun, M. J. Christoe, D. Esrafilzadeh, F.-M. Allieux, M. B. Ghasemian, J. Yang, J. Tang, T. Daeneke, S. Mettu, J. Zhang, M. H. Uddin, R. Jalili and K. Kalantar-Zadeh, *Adv. Funct. Mater.*, 2021, **31**, 2007336.

- 47 S. Merhebi, M. Mayyas, R. Abbasi, M. J. Christoe, J. Han, J. Tang, M. A. Rahim, J. Yang, T. T. Tan, D. Chu, J. Zhang, S. Li, C. H. Wang, K. Kalantar-Zadeh and F.-M. Allieux, *ACS Appl. Mater. Interfaces*, 2020, **12**, 20119–20128.
- 48 S.-Y. Tang, C. Tabor, K. Kalantar-Zadeh and M. D. Dickey, *Annu. Rev. Mater. Res.*, 2021, **51**, 381–408.
- 49 K. Zuraiqi, A. Zavabeti, F.-M. Allieux, J. Tang, C. K. Nguyen, P. Tafazolymotie, M. Mayyas, A. V. Ramarao, M. Spencer, K. Shah, C. F. McConville, K. Kalantar-Zadeh, K. Chiang and T. Daeneke, *Joule*, 2020, **4**, 2290–2321.
- 50 A. Zavabeti, J. Z. Ou, B. J. Carey, N. Syed, R. Orrell-Trigg, E. L. H. Mayes, C. Xu, O. Kavehei, A. P. O'Mullane, R. B. Kaner, K. Kalantar-zadeh and T. Daeneke, *Science*, 2017, **358**, 332–335.
- 51 M. Wurdack, T. Yun, E. Estrecho, N. Syed, S. Bhattacharyya, M. Pieczarka, A. Zavabeti, S.-Y. Chen, B. Haas, J. Müller, M. N. Lockrey, Q. Bao, C. Schneider, Y. Lu, M. S. Fuhrer, A. G. Truscott, T. Daeneke and E. A. Ostrovskaya, *Adv. Mater.*, 2021, **33**, 2005732.
- 52 A. Goff, P. Aukarasereenont, C. K. Nguyen, R. Grant, N. Syed, A. Zavabeti, A. Elbourne and T. Daeneke, *Dalton Trans.*, 2021, **50**, 7513–7526.
- 53 A. Dobosz, Y. Plevachuk, V. Sklyarchuk, B. Sokoliuk and T. Gancarz, *Fluid Phase Equilib.*, 2018, **465**, 1–9.
- 54 A. Dobosz, Y. Plevachuk, V. Sklyarchuk, B. Sokoliuk, O. Tkach and T. Gancarz, *J. Mol. Liq.*, 2018, **271**, 942–948.
- 55 R. S. Datta, N. Syed, A. Zavabeti, A. Jannat, M. Mohiuddin, M. Rokunuzzaman, B. Yue Zhang, M. A. Rahman, P. Atkin, K. A. Messalea, M. B. Ghasemian, E. D. Gaspera, S. Bhattacharyya, M. S. Fuhrer, S. P. Russo, C. F. McConville, D. Esrafilzadeh, K. Kalantar-Zadeh and T. Daeneke, *Nat. Electron.*, 2020, **3**, 51–58.
- 56 M. B. Ghasemian, A. Zavabeti, M. Mousavi, B. J. Murdoch, A. J. Christofferson, N. Meftahi, J. Tang, J. Han, R. Jalili, F.-M. Allieux, M. Mayyas, Z. Chen, A. Elbourne, C. F. McConville, S. P. Russo, S. Ringer and K. Kalantar-Zadeh, *Adv. Mater.*, 2021, **33**, 2104793.
- 57 K. A. Messalea, N. Syed, A. Zavabeti, M. Mohiuddin, A. Jannat, P. Aukarasereenont, C. K. Nguyen, M. X. Low, S. Walia, B. Haas, C. T. Koch, N. Mahmood, K. Khoshmanesh, K. Kalantar-Zadeh and T. Daeneke, *ACS Nano*, 2021, **15**, 16067–16075.
- 58 Z. Hu, T. Yuan, H. Li, Y. Qiu, W. Zhou, J. Zhang, Y. Zhao and S. Hu, *Nano Res.*, 2021, **14**, 4795–4801.
- 59 T. Yuan, Z. Hu, Y. Zhao, J. Fang, J. Lv, Q. Zhang, Z. Zhuang, L. Gu and S. Hu, *Nano Lett.*, 2020, **20**, 2916–2922.
- 60 J. Crawford, A. Cowman and A. P. O'Mullane, *RSC Adv.*, 2020, **10**, 29181–29186.
- 61 T. Alkathiri, N. Dhar, A. Jannat, N. Syed, M. Mohiuddin, M. M. Y. A. Alsaif, R. S. Datta, K. A. Messalea, B. Y. Zhang, M. W. Khan, A. Elbourne, N. Pillai, J. Z. Ou, A. Zavabeti and T. Daeneke, *Chem. Commun.*, 2020, **56**, 4914–4917.
- 62 V. Kochat, A. Samanta, Y. Zhang, S. Bhowmick, P. Manimunda, S. A. S. Asif, A. S. Stender, R. Vajtai, A. K. Singh, C. S. Tiwary and P. M. Ajayan, *Sci. Adv.*, 2018, **4**, e1701373.
- 63 J. Li, X. Zhang, B. Yang, C. Zhang, T. Xu, L. Chen, L. Yang, X. Jin and B. Liu, *Chem. Mater.*, 2021, **33**, 4568–4577.
- 64 K. Vimalanathan, T. Palmer, Z. Gardner, I. Ling, S. Rahpeima, S. Elmas, J. R. Gascooke, C. T. Gibson, Q. Sun, J. Zou, M. R. Andersson, N. Darwish and C. L. Raston, *Nanoscale Adv.*, 2021, **3**, 5785–5792.
- 65 Q. Li, J. Lin, T.-Y. Liu, X.-Y. Zhu, W.-H. Yao and J. Liu, *npj 2D Mater. Appl.*, 2021, **5**, 36.
- 66 J. Cooke, L. Ghadbeigi, R. Sun, A. Bhattacharyya, Y. Wang, M. A. Scarpulla, S. Krishnamoorthy and B. Sensale-Rodriguez, *Phys. Status Solidi A*, 2020, **217**, 1901007.
- 67 R. Lin, W. Zheng, D. Zhang, Y. Li and F. Huang, *ACS Appl. Electron. Mater.*, 2019, **1**, 2166–2173.
- 68 J. Lin, Q. Li, T.-Y. Liu, Y. Cui, H. Zheng and J. Liu, *Phys. Status Solidi RRL*, 2019, **13**, 1900271.
- 69 S.-Y. Tang, V. Sivan, K. Khoshmanesh, A. P. O'Mullane, X. Tang, B. Gol, N. Eshtiaghi, F. Lieder, P. Petersen, A. Mitchell and K. Kalantar-zadeh, *Nanoscale*, 2013, **5**, 5949–5957.
- 70 M. B. Ghasemian, M. Mayyas, S. A. Idrus-Saidi, M. A. Jamal, J. Yang, S. S. Mofarah, E. Adabifiroozjaei, J. Tang, N. Syed, A. P. O'Mullane, T. Daeneke and K. Kalantar-Zadeh, *Adv. Funct. Mater.*, 2019, **29**, 1901649.
- 71 Y. Wang, M. Mayyas, J. Yang, J. Tang, M. B. Ghasemian, J. Han, A. Elbourne, T. Daeneke, R. B. Kaner and K. Kalantar-Zadeh, *Adv. Funct. Mater.*, 2021, **31**, 2005866.
- 72 M. Mousavi, M. B. Ghasemian, J. Han, Y. Wang, R. Abbasi, J. Yang, J. Tang, S. A. Idrus-Saidi, X. Guan, M. J. Christoe, S. Merhebi, C. Zhang, J. Tang, R. Jalili, T. Daeneke, T. Wu, K. Kalantar-Zadeh and M. Mayyas, *Appl. Mater. Today*, 2021, **22**, 100954.
- 73 X. Zhang, L. Xu, J. Zhou, W. Zheng, H. Jiang, K. Zuraiqi, G. K. Li, J. Liu and A. Zavabeti, *ACS Appl. Nano Mater.*, 2021, **4**, 9200–9212.
- 74 Y. Fuseya, H. Katsuno, K. Behnia and A. Kapitulnik, *Nat. Phys.*, 2021, **17**, 1031–1036.
- 75 W.-T. Koo, J. E. Millstone, P. S. Weiss and I.-D. Kim, *ACS Nano*, 2020, **14**, 6407–6413.
- 76 P.-C. Chen, X. Liu, J. L. Hedrick, Z. Xie, S. Wang, Q.-Y. Lin, M. C. Hersam, V. P. Dravid and C. A. Mirkin, *Science*, 2016, **352**, 1565–1569.
- 77 P.-C. Chen, M. Liu, J. S. Du, B. Meckes, S. Wang, H. Lin, V. P. Dravid, C. Wolverton and C. A. Mirkin, *Science*, 2019, **363**, 959–964.
- 78 P. Ferrari, G. Sanzone, J. Yin and E. Janssens, *Chapter 1 – Physical Synthesis of Nanoalloys*, Elsevier, Oxford, 2020.
- 79 Y. Lin, J. Genzer and M. D. Dickey, *Adv. Sci.*, 2020, **7**, 2000192.
- 80 J. Thelen, M. D. Dickey and T. Ward, *Lab Chip*, 2012, **12**, 3961–3967.
- 81 S.-Y. Tang, R. Qiao, Y. Lin, Y. Li, Q. Zhao, D. Yuan, G. Yun, J. Guo, M. D. Dickey, T. J. Huang, T. P. Davis, K. Kalantar-Zadeh and W. Li, *Adv. Mater. Technol.*, 2019, **4**, 1800420.
- 82 I. D. Tevis, L. B. Newcomb and M. Thuo, *Langmuir*, 2014, **30**, 14308–14313.

- 83 M. G. Mohammed, A. Xenakis and M. D. Dickey, *Metals*, 2014, **4**, 465–476.
- 84 S.-Y. Tang, I. D. Joshipura, Y. Lin, K. Kalantar-Zadeh, A. Mitchell, K. Khoshmanesh and M. D. Dickey, *Adv. Mater.*, 2016, **28**, 604–609.
- 85 S. Çınar, I. D. Tevis, J. Chen and M. Thuo, *Sci. Rep.*, 2016, **6**, 21864.
- 86 T. V. Neumann and M. D. Dickey, *Adv. Mater. Technol.*, 2020, **5**, 2000070.
- 87 C. Ladd, J.-H. So, J. Muth and M. D. Dickey, *Adv. Mater.*, 2013, **25**, 5081–5085.
- 88 M. A. Creighton, M. C. Yuen, M. A. Susner, Z. Farrell, B. Maruyama and C. E. Tabor, *Langmuir*, 2020, **36**, 12933–12941.
- 89 Y. Lin, Y. Liu, J. Genzer and M. D. Dickey, *Chem. Sci.*, 2017, **8**, 3832–3837.
- 90 N. Syed, A. Zavabeti, M. Mohiuddin, B. Zhang, Y. Wang, R. S. Datta, P. Atkin, B. J. Carey, C. Tan, J. van Embden, A. S. R. Chesman, J. Z. Ou, T. Daeneke and K. Kalantar-zadeh, *Adv. Funct. Mater.*, 2017, **27**, 1702295.
- 91 S. Cai, M. Mayyas, M. G. Saborio, M. B. Ghasemian, J. Tang, T. Daeneke, J. Han, A. A. Esmailpour, F.-M. Allieux and K. Kalantar-Zadeh, *J. Mater. Chem. C*, 2020, **8**, 16593–16602.
- 92 H. Lu, S.-Y. Tang, Z. Dong, D. Liu, Y. Zhang, C. Zhang, G. Yun, Q. Zhao, K. Kalantar-Zadeh, R. Qiao and W. Li, *ACS Appl. Nano Mater.*, 2020, **3**, 6905–6914.
- 93 S.-Y. Tang, R. Qiao, S. Yan, D. Yuan, Q. Zhao, G. Yun, T. P. Davis and W. Li, *Small*, 2018, **14**, 1800118.
- 94 H. Yu, W. Zhao, L. Ren, H. Wang, P. Guo, X. Yang, Q. Ye, D. Shchukin, Y. Du, S. Dou and H. Wang, *Adv. Mater.*, 2020, **32**, 2001571.
- 95 S. Li, Y. Li, K. Liu, M. Chen, W. Peng, Y. Yang and X. Li, *Appl. Surf. Sci.*, 2021, **565**, 150470.
- 96 J. N. Hohman, M. Kim, G. A. Wadsworth, H. R. Bednar, J. Jiang, M. A. LeThai and P. S. Weiss, *Nano Lett.*, 2011, **11**, 5104–5110.
- 97 F. Hoshyargar, H. Khan, K. Kalantar-zadeh and A. P. O'Mullane, *Chem. Commun.*, 2015, **51**, 14026–14029.
- 98 S. Handschuh-Wang, M. Rauf, T. Gan, W. Shang and X. Zhou, *ChemistrySelect*, 2021, **6**, 10625–10636.
- 99 Z. J. Farrell, C. J. Thrasher, A. E. Flynn and C. E. Tabor, *ACS Appl. Nano Mater.*, 2020, **3**, 6297–6303.
- 100 W. Xie, F.-M. Allieux, R. Namivandi-Zangeneh, M. B. Ghasemian, J. Han, M. A. Rahim, J. Tang, J. Yang, M. Mousavi, M. Mayyas, Z. Cao, F. Centurion, M. J. Christoe, C. Zhang, Y. Wang, S. Merhebi, M. Baharfar, G. Ng, D. Esrafilzadeh, C. Boyer and K. Kalantar-Zadeh, *ACS Nano*, 2021, **15**, 16839–16850.
- 101 S. A. Chechetka, Y. Yu, X. Zhen, M. Pramanik, K. Pu and E. Miyako, *Nat. Commun.*, 2017, **8**, 15432.
- 102 Z. J. Farrell and C. Tabor, *Langmuir*, 2018, **34**, 234–240.
- 103 F. Centurion, M. G. Saborio, F.-M. Allieux, S. Cai, M. B. Ghasemian, K. Kalantar-Zadeh and M. A. Rahim, *Chem. Commun.*, 2019, **55**, 11291–11294.
- 104 Z. J. Farrell, N. Reger, I. Anderson, E. Gawalt and C. Tabor, *J. Phys. Chem. C*, 2018, **122**, 26393–26400.
- 105 Y. Lin, J. Genzer, W. Li, R. Qiao, M. D. Dickey and S.-Y. Tang, *Nanoscale*, 2018, **10**, 19871–19878.
- 106 Q. Wei, M. Sun, Z. Wang, J. Yan, R. Yuan, T. Liu, C. Majidi and K. Matyjaszewski, *ACS Nano*, 2020, **14**, 9884–9893.
- 107 D. Xu, J. Hu, X. Pan, S. Sánchez, X. Yan and X. Ma, *ACS Nano*, 2021, **15**, 11543–11554.
- 108 I. A. de Castro, A. F. Chrimes, A. Zavabeti, K. J. Berean, B. J. Carey, J. Zhuang, Y. Du, S. X. Dou, K. Suzuki, R. A. Shanks, R. Nixon-Luke, G. Bryant, K. Khoshmanesh, K. Kalantar-zadeh and T. Daeneke, *Nano Lett.*, 2017, **17**, 7831–7838.
- 109 H. Okamoto and H. Okamoto, *Phase diagrams for binary alloys*, ASM International, Materials Park, OH, 2000.
- 110 J. Tang, X. Zhao, J. Li, R. Guo, Y. Zhou and J. Liu, *ACS Appl. Mater. Interfaces*, 2017, **9**, 35977–35987.
- 111 D. P. Parekh, C. M. Fancher, M. G. Mohammed, T. V. Neumann, D. Saini, J. Guerrier, C. Ladd, E. Hubbard, J. L. Jones and M. D. Dickey, *ACS Appl. Nano Mater.*, 2020, **3**, 12064–12070.
- 112 D. K. Sarfo, R. R. Taylor and A. P. O'Mullane, *ACS Appl. Electron. Mater.*, 2020, **2**, 2921–2928.
- 113 A. Yamaguchi, Y. Mashima and T. Iyoda, *Angew. Chem., Int. Ed.*, 2015, **54**, 12809–12813.
- 114 V. B. Kumar, Z. e. Porat and A. Gedanken, *J. Therm. Anal. Calorim.*, 2015, **119**, 1587–1592.
- 115 S. A. Idrus-Saidi, J. Tang, M. B. Ghasemian, J. Yang, J. Han, N. Syed, T. Daeneke, R. Abbasi, P. Koshy, A. P. O'Mullane and K. Kalantar-Zadeh, *J. Mater. Chem. A*, 2019, **7**, 17876–17887.
- 116 M. D. Dickey, *Adv. Mater.*, 2017, **29**, 1606425.
- 117 N. Kazem, T. Hellebrekers and C. Majidi, *Adv. Mater.*, 2017, **29**, 1605985.
- 118 A. Fassler and C. Majidi, *Adv. Mater.*, 2015, **27**, 1928–1932.
- 119 M. G. Saborio, S. Cai, J. Tang, M. B. Ghasemian, M. Mayyas, J. Han, M. J. Christoe, S. Peng, P. Koshy, D. Esrafilzadeh, R. Jalili, C. H. Wang and K. Kalantar-Zadeh, *Small*, 2020, **16**, 1903753.
- 120 J. W. Boley, E. L. White and R. K. Kramer, *Adv. Mater.*, 2015, **27**, 2355–2360.
- 121 H. Wang, Y. Yao, Z. He, W. Rao, L. Hu, S. Chen, J. Lin, J. Gao, P. Zhang, X. Sun, X. Wang, Y. Cui, Q. Wang, S. Dong, G. Chen and J. Liu, *Adv. Mater.*, 2019, **31**, 1901337.
- 122 S. Liu, S. Y. Kim, K. E. Henry, D. S. Shah and R. Kramer-Bottiglio, *ACS Appl. Mater. Interfaces*, 2021, **13**, 28729–28736.
- 123 S. Liu, S. N. Reed, M. J. Higgins, M. S. Titus and R. Kramer-Bottiglio, *Nanoscale*, 2019, **11**, 17615–17629.
- 124 G. Yun, S.-Y. Tang, Q. Zhao, Y. Zhang, H. Lu, D. Yuan, S. Sun, L. Deng, M. D. Dickey and W. Li, *Matter*, 2020, **3**, 824–841.
- 125 M. Liao, H. Liao, J. Ye, P. Wan and L. Zhang, *ACS Appl. Mater. Interfaces*, 2019, **11**, 47358–47364.
- 126 J. Xu, Z. Wang, J. You, X. Li, M. Li, X. Wu and C. Li, *Chem. Eng. J.*, 2020, **392**, 123788.
- 127 J.-E. Park, H. S. Kang, J. Baek, T. H. Park, S. Oh, H. Lee, M. Koo and C. Park, *ACS Nano*, 2019, **13**, 9122–9130.

- 128 Z. Zhang, L. Tang, C. Chen, H. Yu, H. Bai, L. Wang, M. Qin, Y. Feng and W. Feng, *J. Mater. Chem. A*, 2021, **9**, 875–883.
- 129 P. Zhang, Q. Wang, R. Guo, M. Zhang, S. Wang, C. Lu, M. Xue, J. Fan, Z. He and W. Rao, *Mater. Horiz.*, 2019, **6**, 1643–1653.
- 130 L. Tang, L. Wang, X. Yang, Y. Feng, Y. Li and W. Feng, *Prog. Mater. Sci.*, 2021, **115**, 100702.
- 131 Y. Jin, Y. Lin, A. Kiani, I. D. Joshipura, M. Ge and M. D. Dickey, *Nat. Commun.*, 2019, **10**, 4187.
- 132 L. Wang and Q. Li, *Chem. Soc. Rev.*, 2018, **47**, 1044–1097.
- 133 T. Gan, S. Handschuh-Wang, W. Shang, J. Shen, L. Zhu, Q. Xiao, S. Hu and X. Zhou, *Macromol. Rapid Commun.*, 2019, **40**, 1900537.
- 134 X. Li, M. Li, Q. Shou, L. Zhou, A. Ge, D. Pei and C. Li, *Adv. Mater.*, 2020, **32**, 2003553.
- 135 F. Centurion, R. Namivandi-Zangeneh, N. Flores, M. Tajik, S. Merhebi, R. Abbasi, M. Mayyas, F.-M. Allieux, J. Tang, W. A. Donald, C. Boyer, M. D. Dickey, K. Kalantar-Zadeh and M. A. Rahim, *ACS Appl. Nano Mater.*, 2021, **4**, 2987–2998.
- 136 F. Hoshyargar, J. Crawford and A. P. O'Mullane, *J. Am. Chem. Soc.*, 2017, **139**, 1464–1471.
- 137 H. Li, R. Abbasi, Y. Wang, F. M. Allieux, P. Koshy, S. A. Idrus-Saidi, M. A. Rahim, J. Yang, M. Mousavi, J. Tang, M. B. Ghasemian, R. Jalili, K. Kalantar-Zadeh and M. Mayyas, *J. Mater. Chem. C*, 2020, **8**, 1656–1665.
- 138 J. Han, J. Yang, J. Tang, M. B. Ghasemian, L. J. Hubble, N. Syed, T. Daeneke and K. Kalantar-Zadeh, *J. Mater. Chem. C*, 2019, **7**, 6375–6382.
- 139 Y. Wang, S. Wang, H. Chang and W. Rao, *Adv. Mater. Interfaces*, 2020, **7**, 2000626.
- 140 M. A. Creighton, M. C. Yuen, N. J. Morris and C. E. Tabor, *Nanoscale*, 2020, **12**, 23995–24005.
- 141 Y. Liu, Q. Wang, J. Deng and W. Zhang, *Chem. Commun.*, 2020, **56**, 1851–1854.
- 142 R. Chen, Q. Xiong, R.-Z. Song, K.-L. Li, Y.-X. Zhang, C. Fang and J.-L. Guo, *Adv. Mater. Interfaces*, 2019, **6**, 1901057.
- 143 X. Tang, S.-Y. Tang, V. Sivan, W. Zhang, A. Mitchell, K. Kalantar-zadeh and K. Khoshmanesh, *Appl. Phys. Lett.*, 2013, **103**, 174104.
- 144 Y.-G. Park, H. Min, H. Kim, A. Zhexembekova, C. Y. Lee and J.-U. Park, *Nano Lett.*, 2019, **19**, 4866–4872.
- 145 C. Zhang, L. Li, X. Yang, J. Shi, L. Gui and J. Liu, *Int. J. Heat Mass Transfer*, 2020, **148**, 119055.
- 146 L. Cao, H. Park, G. Dodbiba, K. Ono, C. Tokoro and T. Fujita, *Appl. Phys. Lett.*, 2011, **99**, 143120.
- 147 W. Kong, Z. Wang, M. Wang, K. C. Manning, A. Uppal, M. D. Green, R. Y. Wang and K. Rykaczewski, *Adv. Mater.*, 2019, **31**, 1904309.
- 148 C. Wei, H. Fei, Y. Tian, Y. An, G. Zeng, J. Feng and Y. Qian, *Small*, 2019, **15**, 1903214.
- 149 P. Won, S. Jeong, C. Majidi and S. H. Ko, *iScience*, 2021, **24**, 102698.
- 150 Y. Lin, C. Cooper, M. Wang, J. J. Adams, J. Genzer and M. D. Dickey, *Small*, 2015, **11**, 6397–6403.
- 151 M. J. Ford, C. P. Ambulo, T. A. Kent, E. J. Markvicka, C. Pan, J. Malen, T. H. Ware and C. Majidi, *Proc. Natl. Acad. Sci. U. S. A.*, 2019, **116**, 21438–21444.
- 152 M. D. Dickey, R. C. Chiechi, R. J. Larsen, E. A. Weiss, D. A. Weitz and G. M. Whitesides, *Adv. Funct. Mater.*, 2008, **18**, 1097–1104.
- 153 G. J. Abbaschian, *J. Less-Common Met.*, 1975, **40**, 329–333.
- 154 T. H. Park, J.-H. Kim and S. Seo, *Adv. Funct. Mater.*, 2020, **30**, 2003694.
- 155 Y.-G. Park, H. S. An, J.-Y. Kim and J.-U. Park, *Sci. Adv.*, 2019, **5**, eaaw2844.
- 156 M.-g. Kim, D. K. Brown and O. Brand, *Nat. Commun.*, 2020, **11**, 1002.
- 157 F.-M. Allieux, J. Han, J. Tang, S. Merhebi, S. Cai, J. Tang, R. Abbasi, F. Centurion, M. Mousavi, C. Zhang, W. Xie, M. Mayyas, M. A. Rahim, M. B. Ghasemian and K. Kalantar-Zadeh, *ACS Appl. Mater. Interfaces*, 2021, **13**, 43247–43257.
- 158 R. C. Chiechi, E. A. Weiss, M. D. Dickey and G. M. Whitesides, *Angew. Chem., Int. Ed.*, 2008, **47**, 142–144.
- 159 R. Tutika, S. H. Zhou, R. E. Napolitano and M. D. Bartlett, *Adv. Funct. Mater.*, 2018, **28**, 1804336.
- 160 R. Guo, X. Wang, H. Chang, W. Yu, S. Liang, W. Rao and J. Liu, *Adv. Eng. Mater.*, 2018, **20**, 1800054.
- 161 M. Tavakoli, M. H. Malakooti, H. Paisana, Y. Ohm, D. Green Marques, P. Alhais Lopes, A. P. Piedade, A. T. de Almeida and C. Majidi, *Adv. Mater.*, 2018, **30**, 1801852.
- 162 U. Daalkhaijav, O. D. Yirmibesoglu, S. Walker and Y. Mengüç, *Adv. Mater. Technol.*, 2018, **3**, 1700351.
- 163 Q. Zhang, Y. Gao and J. Liu, *Appl. Phys. A: Mater. Sci. Process.*, 2014, **116**, 1091–1097.
- 164 J. L. Melcher, K. S. Elassy, R. C. Ordonez, C. Hayashi, A. T. Ohta and D. Garmire, *Micromachines*, 2019, **10**, 54.
- 165 A. Sahlberg, F. Nilsson, A. Berglund, H. Nguyen, K. Hjort and S. H. Jeong, *Adv. Mater. Technol.*, 2018, **3**, 1700330.
- 166 L. Ren, J. Zhuang, G. Casillas, H. Feng, Y. Liu, X. Xu, Y. Liu, J. Chen, Y. Du, L. Jiang and S. X. Dou, *Adv. Funct. Mater.*, 2016, **26**, 8111–8118.
- 167 T. V. Neumann, B. Kara, Y. Sargolzaeiaval, S. Im, J. Ma, J. Yang, M. C. Ozturk and M. D. Dickey, *Micromachines*, 2021, **12**, 146.
- 168 S. Liu, D. S. Shah and R. Kramer-Bottiglio, *Nat. Mater.*, 2021, **20**, 851–858.
- 169 F. Ongul, S. A. Yuksel, S. Bozar, G. Cakmak, H. Y. Guney, D. A. M. Egbe and S. Gunes, *J. Phys. D: Appl. Phys.*, 2015, **48**, 175102.
- 170 K. Chu, B. G. Song, H.-I. Yang, D.-M. Kim, C. S. Lee, M. Park and C.-M. Chung, *Adv. Funct. Mater.*, 2018, **28**, 1800110.
- 171 X. Li, M. Li, L. Zong, X. Wu, J. You, P. Du and C. Li, *Adv. Funct. Mater.*, 2018, **28**, 1804197.
- 172 R. Abbasi, M. Mayyas, M. B. Ghasemian, F. Centurion, J. Yang, M. Saborio, F.-M. Allieux, J. Han, J. Tang, M. J. Christoe, K. M. Mohibul Kabir, K. Kalantar-Zadeh and M. A. Rahim, *J. Mater. Chem. C*, 2020, **8**, 7805–7811.

- 173 B. J. Blaiszik, S. L. B. Kramer, M. E. Grady, D. A. McIlroy, J. S. Moore, N. R. Sottos and S. R. White, *Adv. Mater.*, 2012, **24**, 398–401.
- 174 B. He, Y. Du, B. Wang, X. Zhao, S. Liu, Q. Ye and F. Zhou, *Chem. Eng. J.*, 2022, **427**, 131019.
- 175 N. Kazem, M. D. Bartlett and C. Majidi, *Adv. Mater.*, 2018, **30**, 1706594.
- 176 Y. Xin, J. Lan, J. Xu, D. Wu and J. Zhang, *ACS Appl. Mater. Interfaces*, 2021, **13**, 19351–19359.
- 177 G. Yun, S.-Y. Tang, H. Lu, S. Zhang, M. D. Dickey and W. Li, *Small Sci.*, 2021, **1**, 2000080.
- 178 Y. Peng, H. Liu, T. Li and J. Zhang, *ACS Appl. Mater. Interfaces*, 2020, **12**, 6489–6495.
- 179 J. Yang, D. Tang, J. Ao, T. Ghosh, T. V. Neumann, D. Zhang, Y. Piskarev, T. Yu, V. K. Truong, K. Xie, Y.-C. Lai, Y. Li and M. D. Dickey, *Adv. Funct. Mater.*, 2020, **30**, 2002611.
- 180 G. Bo, H. Yu, L. Ren, N. Cheng, H. Feng, X. Xu, S. X. Dou, H. Wang and Y. Du, *ACS Appl. Nano Mater.*, 2021, **4**, 550–557.
- 181 Y. Yu and E. Miyako, *iScience*, 2018, **3**, 134–148.
- 182 B. Ma, C. Xu, J. Chi, J. Chen, C. Zhao and H. Liu, *Adv. Funct. Mater.*, 2019, **29**, 1901370.
- 183 L. Ren, S. Sun, G. Casillas-Garcia, M. Nancarrow, G. Peleckis, M. Turdy, K. Du, X. Xu, W. Li, L. Jiang, S. X. Dou and Y. Du, *Adv. Mater.*, 2018, **30**, 1802595.
- 184 M. Xiong, Y. Gao and J. Liu, *J. Magn. Magn. Mater.*, 2014, **354**, 279–283.
- 185 L. Cao, D. Yu, Z. Xia, H. Wan, C. Liu, T. Yin and Z. He, *Adv. Mater.*, 2020, **32**, 2000827.
- 186 R. Guo, X. Sun, B. Yuan, H. Wang and J. Liu, *Adv. Sci.*, 2019, **6**, 1901478.
- 187 J.-H. So, J. Thelen, A. Qusba, G. J. Hayes, G. Lazzi and M. D. Dickey, *Adv. Funct. Mater.*, 2009, **19**, 3632–3637.
- 188 K. N. Paracha, A. D. Butt, A. S. Alghamdi, S. A. Babale and P. J. Soh, *Sensors*, 2020, **20**, 177.
- 189 Y. Li, A. Trinchì, W. Włodarski, K. Galatsis and K. Kalantar-zadeh, *Sens. Actuators, B*, 2003, **93**, 431–434.
- 190 M. Ogita, K. Higo, Y. Nakanishi and Y. Hatanaka, *Appl. Surf. Sci.*, 2001, **175–176**, 721–725.
- 191 J. Frank, M. Fleischer and H. Meixner, *Sens. Actuators, B*, 1996, **34**, 373–377.
- 192 M. Shafiei, F. Hoshyargar, N. Motta and A. P. O'Mullane, *Mater. Des.*, 2017, **122**, 288–295.
- 193 Z. Wei, M. K. Akbari, Z. Hai, R. K. Ramachandran, C. Detavernier, F. Verpoort, E. Kats, H. Xu, J. Hu and S. Zhuiykov, *Sens. Actuators, B*, 2019, **287**, 147–156.
- 194 J. Frank, M. Fleischer and H. Meixner, *Sens. Actuators, B*, 1998, **48**, 318–321.
- 195 P. Surmann and H. Zeyat, *Anal. Bioanal. Chem.*, 2005, **383**, 1009–1013.
- 196 J. Zheng, M. A. Rahim, J. Tang, F.-M. Allieux and K. Kalantar-Zadeh, *Adv. Mater. Technol.*, 2021, 2100760.
- 197 W. Zhang, J. Z. Ou, S.-Y. Tang, V. Sivan, D. D. Yao, K. Latham, K. Khoshmanesh, A. Mitchell, A. P. O'Mullane and K. Kalantar-Zadeh, *Adv. Funct. Mater.*, 2014, **24**, 3799–3807.
- 198 Y. Yang, N. Akozbek, T.-H. Kim, J. M. Sanz, F. Moreno, M. Losurdo, A. S. Brown and H. O. Everitt, *ACS Photonics*, 2014, **1**, 582–589.
- 199 J. M. Sanz, D. Ortiz, R. Alcaraz de la Osa, J. M. Saiz, F. González, A. S. Brown, M. Losurdo, H. O. Everitt and F. Moreno, *J. Phys. Chem. C*, 2013, **117**, 19606–19615.
- 200 P. C. Wu, T.-H. Kim, A. S. Brown, M. Losurdo, G. Bruno and H. O. Everitt, *Appl. Phys. Lett.*, 2007, **90**, 103119.
- 201 M. W. Knight, T. Coenen, Y. Yang, B. J. M. Brenny, M. Losurdo, A. S. Brown, H. O. Everitt and A. Polman, *ACS Nano*, 2015, **9**, 2049–2060.
- 202 P. C. Wu, C. G. Khoury, T.-H. Kim, Y. Yang, M. Losurdo, G. V. Bianco, T. Vo-Dinh, A. S. Brown and H. O. Everitt, *J. Am. Chem. Soc.*, 2009, **131**, 12032–12033.
- 203 P. Reineck, Y. Lin, B. C. Gibson, M. D. Dickey, A. D. Greentree and I. S. Maksymov, *Sci. Rep.*, 2019, **9**, 5345.
- 204 A. G. Marín, T. García-Mendiola, C. N. Bernabeu, M. J. Hernández, J. Piqueras, J. L. Pau, F. Pariente and E. Lorenzo, *Nanoscale*, 2016, **8**, 9842–9851.
- 205 P. Albella, B. Garcia-Cueto, F. González, F. Moreno, P. C. Wu, T.-H. Kim, A. Brown, Y. Yang, H. O. Everitt and G. Videen, *Nano Lett.*, 2011, **11**, 3531–3537.
- 206 A. García Marín, M. J. Hernández, E. Ruiz, J. M. Abad, E. Lorenzo, J. Piqueras and J. L. Pau, *Biosens. Bioelectron.*, 2015, **74**, 1069–1075.
- 207 X. Sun, B. Cui, B. Yuan, X. Wang, L. Fan, D. Yu, Z. He, L. Sheng, J. Liu and J. Lu, *Adv. Funct. Mater.*, 2020, **30**, 2003359.
- 208 J. Yan, X. Zhang, Y. Liu, Y. Ye, J. Yu, Q. Chen, J. Wang, Y. Zhang, Q. Hu, Y. Kang, M. Yang and Z. Gu, *Nano Res.*, 2019, **12**, 1313–1320.
- 209 X. Sun, M. Sun, M. Liu, B. Yuan, W. Gao, W. Rao and J. Liu, *Nanoscale*, 2019, **11**, 2655–2667.
- 210 D. Wang, W. Xie, Q. Gao, H. Yan, J. Zhang, J. Lu, B. Liaw, Z. Guo, F. Gao, L. Yin, G. Zhang and L. Zhao, *Small*, 2019, **15**, 1900511.
- 211 J.-J. Hu, M.-D. Liu, F. Gao, Y. Chen, S.-Y. Peng, Z.-H. Li, H. Cheng and X.-Z. Zhang, *Biomaterials*, 2019, **217**, 119303.
- 212 K. Adolfsson, H. Persson, J. Wallentin, S. Oredsson, L. Samuelson, J. O. Tegenfeldt, M. T. Borgström and C. N. Prinz, *Nano Lett.*, 2013, **13**, 4728–4732.
- 213 Q. Liu, T. Yang, Y. Ye, P. Chen, X. Ren, A. Rao, Y. Wan, B. Wang and Z. Luo, *J. Mater. Chem. B*, 2019, **7**, 1442–1449.
- 214 N. Taccardi, M. Grabau, J. Debuschewitz, M. Distaso, M. Brandl, R. Hock, F. Maier, C. Papp, J. Erhard, C. Neiss, W. Peukert, A. Görling, H. P. Steinrück and P. Wasserscheid, *Nat. Chem.*, 2017, **9**, 862–867.
- 215 W. Zhang, B. S. Naidu, J. Z. Ou, A. P. O'Mullane, A. F. Chrimes, B. J. Carey, Y. Wang, S.-Y. Tang, V. Sivan, A. Mitchell, S. K. Bhargava and K. Kalantar-zadeh, *ACS Appl. Mater. Interfaces*, 2015, **7**, 1943–1948.
- 216 O. Oloye, J. D. Riches and A. P. O'Mullane, *Chem. Commun.*, 2021, **57**, 9296–9299.
- 217 J. Tang, J. Tang, M. Mayyas, M. B. Ghasemian, J. Sun, M. A. Rahim, J. Yang, J. Han, D. J. Lawes, R. Jalili, T. Daeneke, Z. Cao, C. A. Echeverria, F.-M. Allieux,



- A. Zavabeti, J. Hamilton, V. Mitchell, A. P. O'Mullane, R. B. Kaner, D. Esrafilzadeh, M. D. Dickey and K. Kalantar-Zadeh, *Adv. Mater.*, 2021, 2105789.
- 218 O. Oloye, C. Tang, A. Du, G. Will and A. P. O'Mullane, *Nanoscale*, 2019, **11**, 9705–9715.
- 219 T. Bauer, S. Maisel, D. Blaumeiser, J. Vecchietti, N. Taccardi, P. Wasserscheid, A. Bonivardi, A. Görling and J. Libuda, *ACS Catal.*, 2019, **9**, 2842–2853.
- 220 Y. Wu, L. Huang, X. Huang, X. Guo, D. Liu, D. Zheng, X. Zhang, R. Ren, D. Qu and J. Chen, *Energy Environ. Sci.*, 2017, **10**, 1854–1861.
- 221 K. T. Lee, Y. S. Jung and S. M. Oh, *J. Am. Chem. Soc.*, 2003, **125**, 5652–5653.
- 222 C. J. Wen and R. A. Huggins, *J. Electrochem. Soc.*, 1981, **128**, 1636–1641.
- 223 S. Zhang, Y. Liu, Q. Fan, C. Zhang, T. Zhou, K. Kalantar-Zadeh and Z. Guo, *Energy Environ. Sci.*, 2021, **14**, 4177–4202.
- 224 R. D. Deshpande, J. Li, Y.-T. Cheng and M. W. Verbrugge, *J. Electrochem. Soc.*, 2011, **158**, A845.
- 225 Y. Jin, K. Liu, J. Lang, D. Zhuo, Z. Huang, C.-A. Wang, H. Wu and Y. Cui, *Nat. Energy*, 2018, **3**, 732–738.
- 226 H. Kim, D. A. Boysen, J. M. Newhouse, B. L. Spatocco, B. Chung, P. J. Burke, D. J. Bradwell, K. Jiang, A. A. Tomaszowska, K. Wang, W. Wei, L. A. Ortiz, S. A. Barriga, S. M. Poizeau and D. R. Sadoway, *Chem. Rev.*, 2013, **113**, 2075–2099.
- 227 Y. Ding, X. Guo, Y. Qian, L. Xue, A. Dolocan and G. Yu, *Adv. Mater.*, 2020, **32**, 2002577.
- 228 G. Liu, J. Y. Kim, M. Wang, J.-Y. Woo, L. Wang, D. Zou and J. K. Lee, *Adv. Energy Mater.*, 2018, **8**, 1703652.
- 229 Y. Wang, X. Wang, M. Xue, Q. Li, Y. Zhang, D. Liu, J. Liu and W. Rao, *Chem. Eng. J.*, 2021, **409**, 128160.
- 230 D. Liu, L. Su, J. Liao, B. Reejayayan and C. Majidi, *Adv. Energy Mater.*, 2019, **9**, 1902798.
- 231 J. Yun, Y. Lim, H. Lee, G. Lee, H. Park, S. Y. Hong, S. W. Jin, Y. H. Lee, S.-S. Lee and J. S. Ha, *Adv. Funct. Mater.*, 2017, **27**, 1700135.
- 232 M.-g. Kim, B. Lee, M. Li, S. Noda, C. Kim, J. Kim, W.-J. Song, S. W. Lee and O. Brand, *ACS Nano*, 2020, **14**, 5659–5667.
- 233 X. Guo, Y. Ding, L. Xue, L. Zhang, C. Zhang, J. B. Goodenough and G. Yu, *Adv. Funct. Mater.*, 2018, **28**, 1804649.
- 234 B. Han, Y. Yang, X. Shi, G. Zhang, L. Gong, D. Xu, H. Zeng, C. Wang, M. Gu and Y. Deng, *Nano Energy*, 2018, **50**, 359–366.
- 235 M. Zhu, S. Li, B. Li and S. Yang, *Nanoscale*, 2019, **11**, 412–417.
- 236 Y. Liu, L.-P. Yue, P. Lou, G.-H. Xu, J. Liang, P. Guo, J. Wang, R. Tao, Y.-C. Cao and L. Shi, *Mater. Lett.*, 2020, **258**, 126803.
- 237 G. Zhang, H. Deng, R. Tao, B. Xiao, T. Hou, S. Yue, N. Shida, Q. Cheng, W. Zhang and J. Liang, *Mater. Lett.*, 2020, **262**, 127194.
- 238 C. Huang, X. Wang, Q. Cao, D. Zhang and J.-Z. Jiang, *ACS Appl. Energy Mater.*, 2021, **4**, 12224–12231.
- 239 J. Zhu, Y. Wu, X. Huang, L. Huang, M. Cao, G. Song, X. Guo, X. Sui, R. Ren and J. Chen, *Nano Energy*, 2019, **62**, 883–889.
- 240 M. Zadan, M. H. Malakooti and C. Majidi, *ACS Appl. Mater. Interfaces*, 2020, **12**, 17921–17928.
- 241 V. Vallem, Y. Sargolzaeiaval, M. Ozturk, Y.-C. Lai and M. D. Dickey, *Adv. Mater.*, 2021, **33**, 2004832.
- 242 F. Suarez, D. P. Parekh, C. Ladd, D. Vashae, M. D. Dickey and M. C. Öztürk, *Appl. Energy*, 2017, **202**, 736–745.
- 243 V. Vallem, E. Roosa, T. Ledinh, W. Jung, T.-I. Kim, S. Rashid-Nadimi, A. Kiani and M. D. Dickey, *Adv. Mater.*, 2021, **33**, 2103142.
- 244 Y. Gao and J. Liu, *Appl. Phys. A: Mater. Sci. Process.*, 2012, **107**, 701–708.
- 245 P. Fan, Z. Sun, Y. Wang, H. Chang, P. Zhang, S. Yao, C. Lu, W. Rao and J. Liu, *RSC Adv.*, 2018, **8**, 16232–16242.
- 246 J. Mingear, Z. Farrell, D. Hartl and C. Tabor, *Nanoscale*, 2021, **13**, 730–738.
- 247 N. Hallfors, A. Khan, M. D. Dickey and A. M. Taylor, *Lab Chip*, 2013, **13**, 522–526.
- 248 W. Xie, F.-M. Allieux, J. Z. Ou, E. Miyako, S.-Y. Tang and K. Kalantar-Zadeh, *Trends Biotechnol.*, 2021, **39**, 624–640.
- 249 P. Zhu, S. Gao, H. Lin, X. Lu, B. Yang, L. Zhang, Y. Chen and J. Shi, *Nano Lett.*, 2019, **19**, 2128–2137.
- 250 Q. Wu, N. Xia, D. Long, L. Tan, W. Rao, J. Yu, C. Fu, X. Ren, H. Li, L. Gou, P. Liang, J. Ren, L. Li and X. Meng, *Nano Lett.*, 2019, **19**, 5277–5286.
- 251 J.-H. Kim, S. Kim, J.-H. So, K. Kim and H.-J. Koo, *ACS Appl. Mater. Interfaces*, 2018, **10**, 17448–17454.
- 252 J. E. Chandler, H. H. Messer and G. Ellender, *J. Dent. Res.*, 1994, **73**, 1554–1559.
- 253 H. Quezada, M. Martínez-Vázquez, E. López-Jácome, B. González-Pedrajo, Á. Andrade, A. M. Fernández-Presas, A. Tovar-García and R. García-Contreras, *Expert Rev. Anti-Infect. Ther.*, 2020, **18**, 609–612.
- 254 L. C. S. Antunes, F. Imperi, F. Minandri and P. Visca, *Antimicrob. Agents Chemother.*, 2012, **56**, 5961–5970.
- 255 S. Hijazi, D. Visaggio, M. Pirolo, E. Frangipani, L. Bernstein and P. Visca, *Front. Cell. Infect. Microbiol.*, 2018, **8**, 316.
- 256 C. H. Goss, Y. Kaneko, L. Khuu, G. D. Anderson, S. Ravishankar, M. L. Aitken, N. Lechtzin, G. Zhou, D. M. Czyz, K. McLean, O. Olakanmi, H. A. Shuman, M. Teresi, E. Wilhelm, E. Caldwell, S. J. Salipante, D. B. Hornick, R. J. Siehnel, L. Becker, B. E. Britigan and P. K. Singh, *Sci. Transl. Med.*, 2018, **10**, eaat7520.
- 257 Z. Xu, X. Zhao, X. Chen, Z. Chen and Z. Xia, *RSC Adv.*, 2017, **7**, 52266–52273.
- 258 L. Kostakoglu, J. P. Leonard, I. Kuji, M. Coleman, S. Vallabhajosula and S. J. Goldsmith, *Cancer*, 2002, **94**, 879–888.
- 259 C. S. Ivanoff, A. E. Ivanoff and T. L. Hottel, *Food Chem. Toxicol.*, 2012, **50**, 212–215.
- 260 K. J. Cummings, M. Nakano, K. Omae, K. Takeuchi, T. Chonan, Y.-L. Xiao, R. A. Harley, V. L. Roggli, A. Hebisawa, R. J. Tallaksen, B. C. Trapnell, G. A. Day,

- R. Saito, M. L. Stanton, E. Suarathana and K. Kreiss, *Chest*, 2012, **141**, 1512–1521.
- 261 Y. Lu, Y. Lin, Z. Chen, Q. Hu, Y. Liu, S. Yu, W. Gao, M. D. Dickey and Z. Gu, *Nano Lett.*, 2017, **17**, 2138–2145.
- 262 Z. Guo, J. Lu, D. Wang, W. Xie, Y. Chi, J. Xu, N. Takuya, J. Zhang, W. Xu, F. Gao, H. Wu and L. Zhao, *Bioact. Mater.*, 2021, **6**, 602–612.
- 263 N. Yang, F. Gong, Y. Zhou, Y. Hao, Z. Dong, H. Lei, L. Zhong, X. Yang, X. Wang, Y. Zhao, Z. Liu and L. Cheng, *Biomaterials*, 2021, **277**, 121125.
- 264 T. Liu, Y. Song, Z. Huang, X. Pu, Y. Wang, G. Yin, L. Gou, J. Weng and X. Meng, *Colloids Surf., B*, 2021, **207**, 112023.
- 265 D. Wang, Q. Wu, R. Guo, C. Lu, M. Niu and W. Rao, *Nanoscale*, 2021, **13**, 8817–8836.
- 266 K. Y. Kwon, S. Cheeseman, A. Frias-De-Diego, H. Hong, J. Yang, W. Jung, H. Yin, B. J. Murdoch, F. Scholle, N. Crook, E. Crisci, M. D. Dickey, V. K. Truong and T.-I. Kim, *Adv. Mater.*, 2021, **33**, 2104298.
- 267 C. B. Eaker and M. D. Dickey, *Appl. Phys. Rev.*, 2016, **3**, 031103.
- 268 J. Liao and C. Majidi, *Soft Matter*, 2021, **17**, 1921–1928.
- 269 G. Li, J. Du, A. Zhang and D.-W. Lee, *J. Appl. Phys.*, 2019, **126**, 084505.
- 270 L. Hu, L. Wang, Y. Ding, S. Zhan and J. Liu, *Adv. Mater.*, 2016, **28**, 9210–9217.
- 271 J. Wissman, M. D. Dickey and C. Majidi, *Adv. Sci.*, 2017, **4**, 1700169.
- 272 S.-Y. Tang, V. Sivan, P. Petersen, W. Zhang, P. D. Morrison, K. Kalantar-zadeh, A. Mitchell and K. Khoshmanesh, *Adv. Funct. Mater.*, 2014, **24**, 5851–5858.
- 273 J. Shu, D.-A. Ge, E. Wang, H. Ren, T. Cole, S.-Y. Tang, X. Li, X. Zhou, R. Li, H. Jin, W. Li, M. D. Dickey and S. Zhang, *Adv. Mater.*, 2021, **33**, 2103062.
- 274 C. Pan, E. J. Markvicka, M. H. Malakooti, J. Yan, L. Hu, K. Matyjaszewski and C. Majidi, *Adv. Mater.*, 2019, **31**, 1900663.
- 275 A. Kotikian, J. M. Morales, A. Lu, J. Mueller, Z. S. Davidson, J. W. Boley and J. A. Lewis, *Adv. Mater.*, 2021, **33**, 2101814.
- 276 Y. Chen, J. Yang, X. Zhang, Y. Feng, H. Zeng, L. Wang and W. Feng, *Mater. Horiz.*, 2021, **8**, 728–757.
- 277 C. P. Ambulo, M. J. Ford, K. Searles, C. Majidi and T. H. Ware, *ACS Appl. Mater. Interfaces*, 2021, **13**, 12805–12813.
- 278 P. Lv, X. Yang, H. K. Bisoyi, H. Zeng, X. Zhang, Y. Chen, P. Xue, S. Shi, A. Priimagi, L. Wang, W. Feng and Q. Li, *Mater. Horiz.*, 2021, **8**, 2475–2484.
- 279 J. Yang, X. Zhang, X. Zhang, L. Wang, W. Feng and Q. Li, *Adv. Mater.*, 2021, **33**, 2004754.
- 280 P. Lv, X. Lu, L. Wang and W. Feng, *Adv. Funct. Mater.*, 2021, **31**, 2104991.
- 281 L. Wang, A. M. Urbas and Q. Li, *Adv. Mater.*, 2020, **32**, 1801335.
- 282 J. Jeon, J. Lee, S. K. Chung and D. Kim, *J. Microelectromech. Syst.*, 2016, **25**, 1050–1057.
- 283 R. Guo, H. Wang, M. Duan, W. Yu, X. Wang and J. Liu, *Smart Mater. Struct.*, 2018, **27**, 085022.
- 284 M. Zhang, P. Zhang, C. Zhang, Y. Wang, H. Chang and W. Rao, *Appl. Mater. Today*, 2020, **19**, 100612.
- 285 D. Yu, Y. Liao, Y. Song, S. Wang, H. Wan, Y. Zeng, T. Yin, W. Yang and Z. He, *Adv. Sci.*, 2020, **7**, 2000177.
- 286 B. Yao, W. Hong, T. Chen, Z. Han, X. Xu, R. Hu, J. Hao, C. Li, H. Li, S. E. Perini, M. T. Lanagan, S. Zhang, Q. Wang and H. Wang, *Adv. Mater.*, 2020, **32**, 1907499.
- 287 M. Zhang, P. Zhang, Q. Wang, L. Li, S. Dong, J. Liu and W. Rao, *J. Mater. Chem. C*, 2019, **7**, 10331–10337.
- 288 Z. Wan, H. Zeng and A. Feinerman, *Appl. Phys. Lett.*, 2006, **89**, 201107.
- 289 K. Nakakubo, H. Yoshioka, K. Morita, R. Ishimatsu, A. Kiani, H. Hallen, M. D. Dickey and Y. Oki, *Opt. Mater. Express*, 2021, **11**, 2099–2108.
- 290 S. Merhebi, M. Mohammad, M. Mayyas, R. Abbasi, C. Zhang, S. Cai, F. Centurion, W. Xie, Z. Cao, J. Tang, M. A. Rahim, J. Zhang, A. Razmjou, G. Leslie, K. Kalantar-Zadeh, J. Tang and F.-M. Allieux, *J. Mater. Chem. A*, 2021, **9**, 19854–19864.
- 291 Y. Gao and Y. Bando, *Nature*, 2002, **415**, 599.
- 292 Z. Liu, Y. Bando, M. Mitome and J. Zhan, *Phys. Rev. Lett.*, 2004, **93**, 095504.
- 293 M. Mayyas, M. Mousavi, M. B. Ghasemian, R. Abbasi, H. Li, M. J. Christoe, J. Han, Y. Wang, C. Zhang, M. A. Rahim, J. Tang, J. Yang, D. Esrafilzadeh, R. Jalili, F.-M. Allieux, A. P. O'Mullane and K. Kalantar-Zadeh, *ACS Nano*, 2020, **14**, 14070–14079.
- 294 B. Lertanantawong, P. Lertsathitphong and A. P. O'Mullane, *Electrochem. Commun.*, 2018, **93**, 15–19.
- 295 M. Mayyas, K. Khoshmanesh, P. Kumar, M. Mousavi, J. Tang, M. B. Ghasemian, J. Yang, Y. Wang, M. Baharfar, M. A. Rahim, W. Xie, F.-M. Allieux, R. Daiyan, R. Jalili, D. Esrafilzadeh and K. Kalantar-Zadeh, *Adv. Funct. Mater.*, 2021, 2108673.
- 296 M. Mayyas, H. Li, P. Kumar, M. B. Ghasemian, J. Yang, Y. Wang, D. J. Lawes, J. Han, M. G. Saborio, J. Tang, R. Jalili, S. H. Lee, W. K. Seong, S. P. Russo, D. Esrafilzadeh, T. Daeneke, R. B. Kaner, R. S. Ruoff and K. Kalantar-Zadeh, *Adv. Mater.*, 2020, **32**, 2001997.
- 297 J. Han, M. Mayyas, J. Tang, M. Mousavi, S. A. Idrus-Saidi, S. Cai, Z. Cao, Y. Wang, J. Tang, R. Jalili, A. P. O'Mullane, R. B. Kaner, K. Khoshmanesh and K. Kalantar-Zadeh, *Matter*, 2021, **4**, 4022–4041.
- 298 M. M. Y. A. Alsaif, S. Kuriakose, S. Walia, N. Syed, A. Jannat, B. Y. Zhang, F. Haque, M. Mohiuddin, T. Alkathiri, N. Pillai, T. Daeneke, J. Z. Ou and A. Zavabeti, *Adv. Mater. Interfaces*, 2019, **6**, 1900007.
- 299 V. Krishnamurthi, T. Ahmed, M. Mohiuddin, A. Zavabeti, N. Pillai, C. F. McConville, N. Mahmood and S. Walia, *Adv. Opt. Mater.*, 2021, 2100449.
- 300 N. Mahmood, H. Khan, K. Tran, P. Kuppe, A. Zavabeti, P. Atkin, M. B. Ghasemian, J. Yang, C. Xu, S. A. Tawfik, M. J. S. Spencer, J. Z. Ou, K. Khoshmanesh, C. F. McConville, Y. Li and K. Kalantar-Zadeh, *Mater. Today*, 2021, **44**, 69–77.
- 301 N. Syed, A. Zavabeti, K. A. Messalea, E. Della Gaspera, A. Elbourne, A. Jannat, M. Mohiuddin, B. Y. Zhang,

- G. Zheng, L. Wang, S. P. Russo, E. Dorna, C. F. McConville, K. Kalantar-Zadeh and T. Daeneke, *J. Am. Chem. Soc.*, 2019, **141**, 104–108.
- 302 B. J. Carey, J. Z. Ou, R. M. Clark, K. J. Berean, A. Zavabeti, A. S. R. Chesman, S. P. Russo, D. W. M. Lau, Z.-Q. Xu, Q. Bao, O. Kavehei, B. C. Gibson, M. D. Dickey, R. B. Kaner, T. Daeneke and K. Kalantar-Zadeh, *Nat. Commun.*, 2017, **8**, 14482.
- 303 M. B. Ghasemian, A. Zavabeti, R. Abbasi, P. V. Kumar, N. Syed, Y. Yao, J. Tang, Y. Wang, A. Elbourne, J. Han, M. Mousavi, T. Daeneke and K. Kalantar-Zadeh, *J. Mater. Chem. A*, 2020, **8**, 19434–19443.